Chemical Engineering Science 338 (2027) 124804

Contents lists available at ScienceDirect

Chemical Engineering Science

journal homepage: www.elsevier.com/locate/ces

# Advanced approximation method with a convergence acceleration parameter for multidimensional aggregation model

Sonia Yadav [a,1], Akashdeep Singh [b,1], Sukhjit Singh [b], Gavin Walker [c], Stefan Heinrich [d], Rohit Ramachandran [e], Mehakpreet Singh [c,f,*]

[a] Department of Mathematics, Jaypee institute of information technology, Noida, India
[b] Department of Mathematics and Computing, Dr. B.R. Ambedkar National Institute of Technology Jalandhar, Punjab 144008, India
[c] Bernal Institute, University of Limerick, Limerick, V94 T9PX, Ireland
[d] Institute of Solids Process Engineering and Particle Technology, Hamburg University of Technology, Denickestraße 15, Hamburg, 21073, Germany
[e] Chemical and Biochemical Engineering, Rutgers University, 98 Brett Road, Piscataway, New Jersey, 08854, USA
[f] Mathematics Applications Consortium for Science and Industry (MACSI), Department of Mathematics and Statistics, University of Limerick, Limerick, V94 T9PX, Ireland

ARTICLE INFO

*2000 MSC:*
34A12
35Q70
45K05
47J35

*Keywords:*
Nonlinear integro-partial differential equation
Convergence acceleration parameter
Existence theorem
Convergence analysis
Finite volume scheme

ABSTRACT

This study presents a highly efficient and accurate approximate method based on a convergence acceleration parameter to approximate a nonlinear multidimensional aggregation population balance equation. Optimal tuning of the acceleration parameter significantly enhances solution quality over extended temporal domains and overcomes key limitations of existing approaches. Deeper mathematical insight is provided through a discussion of the existence of the proposed approach within the framework of a nonlinear aggregation model. Convergence analysis and error estimates are established using the fixed point theorem and the contractive mapping principle, thereby proving the existence of solutions to the aggregation model. The accuracy and efficiency of the proposed approach are demonstrated by computing approximate solutions for the number density function and its moments for physically relevant kernels. For analytically tractable kernels, results are validated against exact solutions. For complex size-dependent kernels, including polymerization, Ruckenstein–Pulvermacher, and shear kernels, the obtained results are compared with the existing finite volume scheme, homotopy analysis method, and optimal decomposition method. The results show that the proposed approach achieves higher accuracy in capturing number density functions and their integral moments while requiring significantly fewer series terms than existing methods.

## 1. Introduction

In a dynamical particulate system, interactions between the particles cause alteration in their physical characteristics such as size, mass, shape or volume. These particulate process are critical to a variety of numerous chemical and colloidal industries deal with the application such as milling process (Wang et al., 2021), food processing industries such as powdered milk, cheese manufacturing in dairy processes (Payens, 1989), granules preparation using fluidized bed granulators and twin screw granulator (Shirazian et al., 2019; Ismail et al., 2020a; Erabit et al., 2016). In addition, raindrop formation (Xue et al., 2008; Briesen, 2006), planet formation (Kobayashi and Tanaka, 2021), and red blood cell aggregation (Ami et al., 2001) are examples of natural science fields where modeling involves analyzing particle interactions, leading to diverse particle properties. These changes taking place within the system due to various mechanisms including nucleation, fragmentation, aggregation, and growth are characterized by the number density function. The primary idea of this work is to deal with the multidimensional aggregation process and mathematically, it is represented by an multidimensional aggregation population balance equation (MAPBE) defined as follows (Filbet and Laurençot, 2004; Matveev et al., 2015; Singh, 2021; Singh et al., 2022a)

$$\frac{\partial \mu(t,\mathbf{y})}{\partial t} = \frac{1}{2}\int_0^{\mathbf{y}} \alpha(\mathbf{y}-\mathbf{w},\mathbf{w})\mu(t,\mathbf{y}-\mathbf{w})\mu(t,\mathbf{w})d\mathbf{w} - \int_0^{\infty} \alpha(\mathbf{y},\mathbf{w})\mu(t,\mathbf{y})\mu(t,\mathbf{w})d\mathbf{w}, \tag{1}$$

* Corresponding author.
*E-mail addresses:* kundalss@nitj.ac.in (S. Singh), Gavin.Walker@ul.ie (G. Walker), stefan.heinrich@tuhh.de (S. Heinrich), rohit.r@rutgers.edu (R. Ramachandran), Mehakpreet.Singh@ul.ie (M. Singh).
[1] Both authors contributed equally.

https://doi.org/10.1016/j.ces.2026.124804
Received 10 February 2026; Received in revised form 22 June 2026; Accepted 30 June 2026
Available online 3 August 2026
0009-2509/© 2026 The Authors. Published by Elsevier Ltd. This is an open access article under the CC BY license (http://creativecommons.org/licenses/by/4.0/).

$$\mu(0,\mathbf{y}) = \mu_0(\mathbf{y}) \geq 0. \tag{2}$$

Here the space of vectors $\mathbf{y} = [y_1, y_2, \ldots, y_n]^T$ of length $n$ in $\mathbb{R}^d_+$, such that $y_n \geq 0$ for all $n = 1, 2, \ldots, d$. For this study, we consider only three properties of the system, that is, $d = 3$. Moreover, $\mu(t, \mathbf{y})$ represents number density function of particle properties $\mathbf{y} = [y_1, y_2, y_3]^T \geq 0$ at time $t$ and the left hand side of Eq. (1) represents the rate of change number density function with respect to time $t$. In right hand side of Eq. (1), the first integral indicates the formation of $\mathbf{y}$ particle property and the second integral represents the removal of $\mathbf{y}$ particle property during the process of aggregation. The aggregation kernel $\alpha(\mathbf{y}, \mathbf{w})$ denotes the rate at which particles properties $\mathbf{y}$ and $\mathbf{w}$ aggregate to form a new particle property $\mathbf{y} + \mathbf{w}$. Generally, the aggregation kernel $\alpha(\mathbf{y}, \mathbf{w})$ is assumed to be a non-negative, and symmetric function on the considered domain. While aggregation leads to a decrease in the total number of particles, the mass remains conserved in both scenarios. As a result, all phenomena are expected to adhere to the principles of mass conservation. Mathematically, it is presented as

$$\int_0^\infty \mathbf{y}\mu(t,\mathbf{y})d\mathbf{y} = \int_0^\infty \mathbf{y}\mu_0(\mathbf{y})d\mathbf{y} \tag{3}$$

The evaluation of fundamental properties such as moments are of special interest due to their physical interpretability. The $k$th moment of the number density function is defined as follows:

$$\nu_{\mathbf{k}}(t) = \int_0^\infty \mathbf{y}^{\mathbf{k}}\mu(t,\mathbf{y})d\mathbf{y} \qquad \text{for} \qquad \mathbf{k} = 0, 1, 2, \ldots$$

This represents various physical properties such as the total number of particles is defined by zeroth order moment and the total number of volume is estimated by the first order moment.

### 1.1. Motivation and the state of art

Given the complex nonlinear nature, it is not always feasible to analytically solve the nonlinear aggregation population balance Eq. (1). Due to the broad range of applications in pharmaceutical and dairy manufacturing, it is essential to investigate the methods for solving the population balance equation corresponding to heavy size-dependent physically relevant kernels. However, high-speed computing has made it easier for researchers to work on solutions for various population balance equations with complex structured kernels. The aggregation model has been solved using a variety of numerical and semi-analytical techniques. Ranjbar et al. (2010) employed the problem using the radial basis function and Taylor polynomials. Marchisio et al. (2003) used the quadrature rule to solve the population balance equation. Different finite volume schemes for solving a aggregation equation have been developed in the literature (Filbet and Laurençot, 2004; Singh et al., 2020; Singh, 2023). Santra et al. (2025) analyzed a multi-dimensional wavelet-based methods with higher-order convergence for approximating weak singularities in nonlocal integro-partial differential equations. In Santra et al. (2023), a stable high-order graded-mesh L1 scheme is presented for solving multi-term time-fractional partial integro-differential equations for initial singularities and sharp layer behavior. Kumar et al. (2024b) investigated the theoretical and numerical effects of mixed flux boundary conditions and nonsmooth data on singularly perturbed semilinear reaction–diffusion problems, establishing nearly second-order uniformly accurate schemes for resolving boundary and interior layers. Saini et al. (2023) developed a computationally efficient triangular-splitting additive method, and achieved uniform first-order accuracy in time and second-order accuracy in space for multiscale coupled parabolic systems with mixed boundary conditions. Das et al. (2020b) presented adaptive moving-mesh and cubic spline-based numerical methods that achieve first- and second-order uniformly accurate approximations, respectively, for singularly perturbed reaction–diffusion systems with mixed boundary conditions and boundary layers. In, Saini et al. (2024), an adaptive moving-mesh finite difference method with second-order parameter-uniform convergence is presented for singularly perturbed parabolic reaction–diffusion problems with Robin boundary conditions and large time delays, outperforming standard upwind schemes. Kumar et al. (2024a) developed adaptive moving-mesh finite difference and finite element methods for efficiently solving Darcy-scale precipitation–dissolution reactive transport models, accurately tracking moving reaction fronts while reducing computational cost in one-dimensional (1D) and two-dimensional (2D) porous media problems. Some other important numerical techniques as sectional discretization (Kumar and Warnecke, 2008), fixed point technique (Giri and Hausenblas, 2013), fast Fourier transformation method (Ahrens and Le Borne, 2018), cell average technique (Mostafaei and Rajabi-Hamane, 2017) and population dynamics algorithm (Gunawan et al., 2004) also available in the literature. The limitations of numerical methods become evident through their potential reliance on non-physical concepts, such as linearization, selection of basis functions, parameter discretization (such as time steps and grid size), and other factors. Singh et al. (2022c,b) offer a thorough examination of the advantages and drawbacks associated with the fixed pivot technique, cell average technique, finite volume schemes, and Monte Carlo methods.

To overcome this, researchers' emphasis is on facilitating the development of a semi-analytical technique. These approaches track the solution as an infinite series form which is a significant advantage over the traditional numerical methods. Hammouch and Mekkaoui (2012) formulated Laplace variational iteration method (LVIM) for obtaining series solution of (1) for the constant and product kernel. Singh et al. (2015) used the Adomian decomposition method (ADM) for the solution of pure aggregation PBE with constant sum and product aggregation kernel. Das et al. (2020a) established the convergence of a homotopy analysis based perturbation method to solve Caputo fractional volterra Fredholm integro differential equations, providing accurate approximations for both standard and higher order problems. Turkyilmazoglu (2016) demonstrated the superiority of the optimal variational iteration method over the classical variational iteration method by establishing convergence with optimal convergence parameter, and successfully applying the method to heat and fluid flow problems. Turkyilmazoglu (2018) presented a modified Adomian decomposition method with a convergence-control parameter that ensures reliable and accurate solutions of nonlinear heat transfer problems, while overcoming the convergence and accuracy limitations of the classical ADM. Turkyilmazoglu (2022) introduced a modified Adomian decomposition method with an optimally determined convergence parameter based on a residual $L^2$-norm approach, providing highly accurate and efficient solutions for fractional ordinary and partial differential equations and outperforming several existing numerical methods. Turkyilmazoglu (2024) demonstrated that incorporating a convergence control parameter into classical iterative methods, including fixed point iteration, the Adomian decomposition method, and the homotopy analysis method, significantly improves convergence and accuracy by enabling the determination of an optimal parameter through residual error minimization.

Recently, Kaur et al. established the Homotopy perturbation method (HPM) (Kaur et al., 2019) and Homotopy analysis method (HAM) Kaur et al. (2022) for approximating the solution of (1) for constant, sum, product and Ruckenstein kernel. They have considered discrete averaged residual errors formula for determining the value of auxiliary convergence-control parameter in HAM. It was noticeable that the HPM accurately tracks the analytical solutions only for a shorter period. To overcome this, Yadav et al. (2023) combined HPM with Pade approximant to improve the results over a longer time domain. Kushwah and Saha (2023) also implemented HAM for the series solution of (1) but they plotted $h$ curves for choosing a suitable value of convergence control parameter and the obtained results are better than existing HPM. Moreover, Arora et al. (2023) performed a comparative study between the variational iteration method (VIM) and ADM for solving the population balance equation. VIM is shown excellent agreement to exact so-

lutions over ADM even by consuming less number of iterative terms. In addition, to solve the growth model and aggregation equation only with a constant kernel, the optimal variational iteration method (OVIM) was used. However, for other relevant kernels, OVIM required a large computational time. In Kaushik and Kumar (2023), authors demonstrated the optimal decomposition method (ODM) to aggregation equation only for constant, sum and product kernel.

Forestier-Coste and Mancini (2012) presents a finite volume scheme for solving the coalescence (Smoluchowski) equation. This method is designed to conserve first-order momentum, handle non-uniform grids, and is generalizable to multidimensional frameworks. Our numerical results are compared with existing literature. Vale and McKenna (2005) extended the fixed pivot technique originally for one-dimensional systems, to simulate two-component aggregation processes, yielding an accurate and computationally efficient numerical method that maintains internal consistency for key moments like number of particles and the mass of each component on arbitrary Cartesian grids. Hussain and Kumar (2024) propose a semi-analytical approach combining the Elzaki integral transform with the projected differential transform method to directly solve multi-dimensional aggregation equations without discretization, demonstrating high accuracy and convergence, with closed-form solutions obtained for aggregation under specific kernels.

Zhang et al. (2018) recently formulated a new approximation method with a convergence control parameter (AMP) for solving nonlinear physical models such as diffusion and dissipation phenomena, nano-electromechanical systems, dispersive waves and heat transfer problems. It turns out that by selecting an appropriate value of a convergence parameter, the convergence region and rate can be significantly improved. This motivates us to adapt the AMP to compute the series solutions for a nonlinear aggregation Eq. (1). The aim of this work is three-fold: (i) construction of mathematical formulation of AMP for a nonlinear aggregation equation (ii) existence theorem and detailed convergence analysis (iii) determining new approximate solutions of the number density functions by AMP for complex polymerization, Ruckenstein/Pulvermacher, and shear kernels corresponding to both exponential and Gamma initial distributions. In order to assess the level of accuracy achieved by the novel approach, a comparison is made with recently employed techniques, such as ODM and HAM.

Motivated by the preceding discussion, this work develops a semi-analytical framework based on the convergence-control parameter method for the solution of nonlinear multidimensional aggregation population balance equations (PBEs). The principal advantages of the proposed approach are summarized as follows:

- A direct recursive scheme is formulated to efficiently compute the components of the series solution.
- It offers approximate solutions for complex polymerization, ruckenstein/pulvermacher, and shear kernels, corresponding to exponential and gamma initial distributions.
- The present approach is more efficient than existing semi-analytical approaches, such as the homotopy analysis method (HAM) Kaur et al. (2022) and the optimal decomposition method (ODM) Kaushik and Kumar (2023), as it require fewer series terms to achieve high accuracy.
- The proposed method accurately captures integral properties, such as the zeroth- and first-order moments demonstrating excellent precision.
- This approach is extended to solve 2D nonlinear aggregation PBEs over longer time intervals and, for the first time, to address three-dimensional nonlinear aggregation PBEs.

The article is structured as follows: Section 2 is devoted to establish the general methodology and formulation of the proposed approach for one and two dimensional nonlinear aggregation equations. In Section 3, the efficiency and accuracy of AMP are presented and compared with ODM and HAM by considering different numerical examples. Section 4 is devoted to made some remarks, conclusions and future studies.

## 2. Approximation method with a convergence acceleration parameter (AMP)

In this section, the overview of the mathematical formulation of the approximation method with a convergence acceleration parameter (AMP) and its adaptability for solving a nonlinear aggregation model are derived.

### 2.1. *Overview of* AMP *methodology*

Let us first derive the mathematical formulation of the AMP for a general nonlinear functional equation

$$\mathcal{L}[\mu] + \mathcal{R}[\mu] + \mathcal{N}[\mu] = g[t, y], \tag{4}$$

with an initial condition $\mu(0, y) = \mu_0(y)$, where $\mathcal{L}$ is generally the highest order linear term that is easily invertible but the choice is not unique. In addition, $\mathcal{R}$, $\mathcal{N}$ and $g(y)$ denote the remainder linear term, nonlinear term and source term, respectively. To begin, a new equation is created by adding an artificial parameter $\upsilon \in [0, 1]$ and a convergence control parameter $p \in \mathbb{R}$ in Eq. (4), we get

$$\mathcal{L}[\mu] + (\upsilon p + \upsilon^2(1-p))(\mathcal{R}[\mu] + \mathcal{N}[\mu]) = g[t, y]. \tag{5}$$

Now, operate $\mathcal{L}^{-1}$ on both side, we have

$$\mu(t, y) = \mu_0(y) - (\upsilon p + \upsilon^2(1-p))\mathcal{L}^{-1}(\mathcal{R}[\mu] + \mathcal{N}[\mu]) + \mathcal{L}^{-1}[g[t, y]]. \tag{6}$$

Next, one sets $\mu(t, y) = \sum_{m=0}^{\infty} \mu_m(t, y, p)\upsilon^m$. A new recurrence relation is generated by substituting value of $\mu$ into (4) and collecting the coefficients of powers of $\upsilon$, we get

$$\begin{aligned}
&\mu_0(t, y, p) = \mu_0 + \mathcal{L}^{-1}[g(y)] \\
&\mu_1(t, y, p) = -p\mathcal{L}^{-1}[\mathcal{R}(\mu_0(t, y, p)) + \mathcal{B}_0] \\
&\mu_m(t, y, p) = -p\mathcal{L}^{-1}[\mathcal{R}(\mu_{m-1}(t, y, p)) + \mathcal{B}_{m-1}] \\
&\qquad\qquad - (1-p)\mathcal{L}^{-1}[\mathcal{R}(\mu_{m-2}(t, y, p)) + \mathcal{B}_{m-2}], \qquad m = 2, 3, \ldots
\end{aligned}$$

where, the coefficient $\mathcal{B}_m = \frac{1}{m!}\left[\frac{d^m}{d\upsilon^m}\mathcal{N}\left(\sum_{n=0}^{\infty}\mu_n(t, y, p)\upsilon^n\right)\right]$.

For $\upsilon = 1$, the solution $\mu(t, y)$ with parameter $p$ is given by

$$\mu(t, y, p) = \sum_{m=0}^{\infty} \mu_m(t, y, p).$$

In addition, the $r$th- order approximation solution is given by

$$\vartheta_r(t, y, p) = \sum_{m=0}^{r} \mu_m(t, y, p), \qquad r \geq 1. \tag{7}$$

Further the optimal value of the convergence acceleration parameter $p$ for the $r$th order approximation (7) is calculated by minimizing the residual error, that is,

$$\min_{p\in\mathbb{R}} G(p), \tag{8}$$

where

$$G(p) = \frac{1}{N^2}\sum_{k=1}^{N}\sum_{j=1}^{N}[(\mathcal{L} + \mathcal{R} + \mathcal{N})(\vartheta_r(\tau_j, y_k, p) - g(y_k)]^2 \tag{9}$$

and $y_1, y_2, \ldots, y_N$, $\tau_1, \tau_2, \ldots, \tau_N$ are the arbitrary points.

### 2.2. AMP *for 1D aggregation PBE*

In this subsection, we enhance the use of approximation method with a convergence acceleration parameter to solve aggregation PBE. By comparing the aggregation PBE (1) with (4), we get

$$\mathcal{L}[\mu] = \frac{\partial\mu}{\partial t}, \quad \mathcal{R}[\mu] = 0, \quad \mathcal{N}[\mu] = -\frac{1}{2}\int_0^y \alpha(y-w, w)\mu(t, y-w)\mu(t, w)dw + \int_0^{\infty} \alpha(y, w)\mu(t, y)\mu(t, w)dw \text{ and } g(t, y) = 0.$$

Denote the nonlinear term in $\mathcal{N}$ by $h_1(\mu) = \mu(t, y-w)\mu(t, w)$ and $h_2(\mu) = \mu(t, y)\mu(t, w)$.

Thus, to apply AMP Eq. (6) can be written as

$$\frac{\partial \mu(t,y)}{\partial t} - (\upsilon p + \upsilon^2(1-p))\left(\frac{1}{2}\int_0^y \alpha(y-w,w)h_1(\mu)dw - \int_0^\infty \alpha(y,w)h_2(\mu)dw\right) = 0. \tag{10}$$

Integrating (10) from 0 to $t$, we get

$$\mu(t,y) = \mu_0(y) + (\upsilon p + \upsilon^2(1-p))\int_0^t \left(\frac{1}{2}\int_0^y \alpha(y-w,w)h_1(\mu)dw - \int_0^\infty \alpha(y,w)h_2(\mu)dw\right)dwdt \tag{11}$$

Substitute $\mu(t,y) = \sum_{m=0}^{\infty} \mu_m(t,y,p)\upsilon^m$ into Eq. (11) and collecting the coefficients of powers of $\upsilon$, we get the following recursive relation

$$\begin{cases} \mu_0(y) \text{ given} \\ \mu_1(t,y,p) = p\int_0^t \left[\frac{1}{2}\int_0^y \alpha(y-w,w)\mathcal{P}_0(\mu)dw - \int_0^\infty \alpha(y,w)\mathcal{Q}_0(\mu)dw\right]dt \\ \mu_m(t,y,p) = (1-p)\int_0^t \left[\frac{1}{2}\int_0^y \alpha(y-w,w)\mathcal{P}_{m-2}(\mu)dw - \int_0^\infty \alpha(y,w)\mathcal{Q}_{m-2}(\mu)dw\right]dt \\ \quad + p\int_0^t \left[\frac{1}{2}\int_0^y \alpha(y-w,w)\mathcal{P}_{m-1}(\mu)dw - \int_0^\infty \alpha(y,w)\mathcal{Q}_{m-1}(\mu)dw\right]dt \end{cases} \tag{12}$$

where $\mathcal{P}_m = \frac{1}{m!}\frac{d^m}{d\upsilon^m}\left[h_1\left(\sum_{n=0}^{\infty}\mu_n\upsilon^n\right)\right]_{\upsilon=0}$ and $\mathcal{Q}_m = \frac{1}{m!}\frac{d^m}{d\upsilon^m}\left[h_2\left(\sum_{n=0}^{\infty}\mu_n\upsilon^n\right)\right]_{\upsilon=0}$.

The $r$th- order approximation solution is given by

$$\vartheta_r(t,y,p) = \sum_{m=0}^{r}\mu_m(t,y,p), \qquad r \geq 1 \tag{13}$$

Following that, for obtaining the optimal value of the convergence acceleration parameter $p$ for the $r$th order approximation (13) is calculated for a nonlienar aggregation equations by minimizing the residual error (8) with

$$G(p) = \frac{1}{N^2}\sum_{k=1}^{N}\sum_{j=1}^{N}\left[\frac{\partial}{\partial t}\vartheta_r(t_j,y_k,p) - \frac{1}{2}\int_0^{y_k}\alpha(y_k-w,w)\vartheta_r(t_j,y_k-w,p)\vartheta_r(t_j,w,p)dw + \int_0^\infty \alpha(y_k,w)\vartheta_r(t_j,y_k,p)\vartheta_r(t_j,w,p)dw\right]^2 \tag{14}$$

and $y_1, y_2, \ldots, y_N, t_1, t_2, \ldots, t_N$ are the arbitrary points.

### 2.3. AMP *for 2D aggregation PBE*

In this subsection, we improve the approximation method by introducing a convergence acceleration parameter to effectively solve the APBE. By comparing the 2D aggregation PBE given in (1) with that in (4), we obtain the following:

$$\mathcal{L}[\mu] = \frac{\partial \mu}{\partial t}, \quad \mathcal{R}[\mu] = 0, \quad g(t,y) = 0, \text{ and}$$

$$\mathcal{N}[\mu] = -\frac{1}{2}\int_0^y\int_0^z \alpha(y-w,w,z-x,x)\mu(t,y-w,z-x)\mu(t,w,x)\,dx\,dw + \int_0^\infty\int_0^\infty \alpha(y,w,z,x)\mu(t,y,z)\mu(t,w,x)\,dx\,dw \tag{15}$$

Denote the nonlinear term in $\mathcal{N}$ by $g_1(\mu) = \mu(t,y-w,z-x)\mu(t,w,x)$ and $g_2(\mu) = \mu(t,y,z)\mu(t,w,x)$.

In order to effectively apply the AMP method, we derive the following expressions as

$$\frac{\partial \mu(t,y,z)}{\partial t} - (\upsilon p + \upsilon^2(1-p))\left(\frac{1}{2}\int_0^y\int_0^z \alpha(y-w,w,z-x,x)\mu(t,y-w,z-x)\mu(t,w,x)\,dx\,dw - \int_0^\infty\int_0^\infty \alpha(y,w,z,x)\mu(t,y,z)\mu(t,w,x)\,dx\,dw\right) = 0. \tag{16}$$

Integrating (16) from 0 to $t$, we get

$$\mu(t,y,z) = \mu_0(y,z) + (\upsilon p + \upsilon^2(1-p))\int_0^t \left(\frac{1}{2}\int_0^y\int_0^z \alpha(y-w,w,z-x,x)g_1(\mu)\,dx\,dw - \int_0^\infty\int_0^\infty \alpha(y,w,z,x)g_2(\mu)\,dx\,dw\right)dt \tag{17}$$

Substitute $\mu(t,y,z) = \sum_{m=0}^{\infty}\mu_m(t,y,z,p)\upsilon^m$ into Eq. (17) and collecting the coefficients of powers of $\upsilon$, we get the following recursive relation

$$\begin{cases} \mu_0(y,z) \quad \text{given} \\ \mu_1(t,y,z,p) = p\int_0^t \left[\frac{1}{2}\int_0^y\int_0^z \alpha(y-w,w,z-x,x)\mathcal{R}_0(\mu)dxdw - \int_0^\infty\int_0^\infty \alpha(y,w,z,x)\mathcal{T}_0(\mu)dxdw\right]dt \\ \mu_m(t,y,z,p) = (1-p)\int_0^t \left[\frac{1}{2}\int_0^y\int_0^z \alpha(y-w,w,z-x,x)\mathcal{R}_{m-2}(\mu)dxdw - \int_0^\infty\int_0^\infty \alpha(y,w,z,x)\mathcal{T}_{m-2}(\mu)dxdw\right]dt \\ \quad + p\int_0^t \left[\frac{1}{2}\int_0^y\int_0^z \alpha(y-w,w,z-x,x)\mathcal{R}_{m-1}(\mu)dxdw - \int_0^\infty\int_0^\infty \alpha(y,w,z,x)\mathcal{T}_{m-1}(\mu)dxdw\right]dt \end{cases} \tag{18}$$

where $\mathcal{R}_m = \frac{1}{m!}\frac{d^m}{d\upsilon^m}\left[g_1\left(\sum_{n=0}^{\infty}\mu_n\upsilon^n\right)\right]_{\upsilon=0}$ and $\mathcal{T}_m = \frac{1}{m!}\frac{d^m}{d\upsilon^m}\left[g_2\left(\sum_{n=0}^{\infty}\mu_n\upsilon^n\right)\right]_{\upsilon=0}$.

The $r$th- order approximation solution is given by

$$\vartheta_r(t,y,z,p) = \sum_{m=0}^{r}\mu_m(t,y,z,p), \qquad r \geq 1 \tag{19}$$

Subsequently, the optimal value of the convergence acceleration parameter $p$ for the $r$th-order approximation, as defined in (19), is determined for the nonlinear aggregation equations by minimizing the residual error is given by

$$G(p) = \frac{1}{N^3}\sum_{i=1}^{N}\sum_{k=1}^{N}\sum_{j=1}^{N}\left[\frac{\partial}{\partial t}\vartheta_r(t_j,y_k,z_i,p)\right.$$

$$-\frac{1}{2}\int_0^{y_k}\int_0^{z_i}\alpha(y_k-w,w,z_i-x,x)\mu(t,y_k-w,z_i-x)\mu(t,w,x)dxdw + \int_0^{\infty}\int_0^{\infty}\alpha(y_k,w,z_i,x)\mu(t,y_k,z_i)\mu(t,w,x)\,dx\,dw\Big]^2 \tag{20}$$

and $y_1, y_2, \ldots, y_N$, $z_1, z_2, \ldots, z_N$, $t_1, t_2, \ldots, t_N$ are the arbitrary points.

## 3. Numerical examples

In this section, the testing of the AMP for pure aggregation Eq. (1) with analytical and physically relevant kernels. We consider different aggregation kernels along with an exponential and Gamma initial distributions. For each kernel, we consider 20 arbitrary points for minimizing residual error defined in (8) to obtain the optimal value of convergence control parameter $p$. For sum and product kernels, the exact solutions of the number density functions exist in the literature. To determine the accuracy of AMP, the series solution is validated by the existing exact solutions for analytical tractable kernels. On the other hand, for complex polymerization, Ruckenstein/Pulvermacher, and shear kernels, the approximate series solution of the number density function and moments are compared with the finite volume scheme (Kumar et al., 2016). It is worth mentioning that the series solutions for the polymerization, Ruckenstein/Pulvermacher, and shear kernels corresponding to a Gamma initial distribution is derived for the first time. Furthermore, the truncation error ($\delta$) between the exact solution $\mu(t,y)$ and the approximation solution $\vartheta_r(t,y)$ is evaluated for iterative methods by using the following relation (Singh et al., 2015):

$$\delta=\sum_{k=1}^{1000}|\vartheta_r^k-\mu_k|l_k,\qquad r=1,2,3,\ldots \tag{21}$$

where $\vartheta_r^k=\vartheta_r(t,y_k)$, $\mu_k=\mu(t,y_k)$. First, we divide the interval $[0,Y]$ into 1000 random intervals $[y_{k-\frac{1}{2}},y_{k+\frac{1}{2}}]$ for $k=0,1,\ldots,1000$. Now, $y_k=\frac{y_{k-\frac{1}{2}}+y_{k+\frac{1}{2}}}{2}$ is the midpoint of the interval and the value of $l_k=y_{k-\frac{1}{2}}-y_{k+\frac{1}{2}}$.

### 3.1. Testing for 1D aggregation equation

To evaluate the accuracy and efficiency of the proposed approach for the 1D aggregation model (1), we considered a wide range of aggregation kernels corresponding to various initial conditions (ICs). The performance of the proposed approach was tested against established existing methods: the homotopy analysis method (HAM) Kaur et al. (2022) and the optimal decomposition method (ODM) Kaushik and Kumar (2023). A key step in this evaluation involved applying all mentioned approaches to the aggregation model allowing for a rigorous, direct comparison to assess their relative efficiency.

#### 3.1.1. Sum kernel $\alpha(y,w)=y+w$ with $\mu_0(y)=e^{-y}$

The analytic solution of (1) for sum $e^{-y}$ kernel with an exponential initial distribution is given by Scott (1968)

$$\mu(t,y)=\frac{(1-\nu(t))e^{-(1+\nu(t))y}}{y\sqrt{\nu(t)}}\mathcal{M}(2y\sqrt{\nu(t)}), \tag{22}$$

where, $\mathcal{M}(t)$ is the modified Bessel function of the first kind and $\nu(t)=1-e^{-t}$. The aggregation of atmospheric particles in dust, soot formation, and aerosols are modeled using the sum kernel (Liu and Rigopoulos, 2019). Other applications of this kernel can be found in batch and continuous granulation processes (Ismail et al., 2020b).

According to AMP, by using iterative formula (12) for sum kernel with $\mu_0(y)=e^{-y}$, we get the following successive iterations

$$\mu_1(t,y,p)=-\frac{pte^{-y}\left(-y^2+2y+2\right)}{2}$$

$$\mu_2(t,y,p)=\frac{p^2t^2e^{-y}\left(y^4-6y^3-3y^2+18y+6\right)}{12}+\frac{pte^{-y}(p-1)\left(-y^2+2y+2\right)}{2}$$

$$\mu_3(t,y,p)=-(p-1)\Big(\frac{p^2t^2e^{-y}\left(y^4-6y^3-3y^2+18y+6\right)}{12}+\frac{pte^{-y}(p-1)\left(-y^2+2y+2\right)}{2}\Big)-\frac{p^2t^2e^{-y}}{144}\big(72p-216y+24pt+216py-36py^2-72py^3+12py^4+36y^2+72y^3-12y^4+60pty^2-120pty^3-12pty^4+12pty^5-pty^6+168pty-72\big)$$

$$\vdots$$

By using the first nine iterative terms, the truncated series solution by AMP is given by

$$\vartheta_9(t,y,p)=p^9t^7y^{13}e^{-y}(t^2y^5-90t^2y^4+2790t^2y^3-28080t^2y^2-204660t^2y+5110560t^2-720ty^3+51840ty^2-1218240ty+7257600t+181440y+\ldots) \tag{23}$$

The TSS (23) is plotted as a function of $p$ for fixed parameters $y=10$ and $t=2$ in Fig. 1a. This plot reveals that the $p$-curve remains relatively constant within the interval $p\in[-0.55,0.85]$. Based on this range, the optimal value of $p$ was chosen to be 0.34. The solutions obtained by AMP after substituting the value of $p$ and $t$ are compared against the exact solutions (22) as depicted in Fig. 1b. As observed, AMP solution matches well with exact solution for shorter ($t=0.5$) as well as longer time ($t=1.5$). On the other hand, by considering $t=1.5$ and same number of iterative terms of HAM and ODM, the number density functions show fluctuation with respect to the exact solution (see Fig. 1c). In addition, zeroth and first order moments by AMP and exact solution are plotted in Fig. 1d. The total number of particles decreases due to the aggregation process and well matched with the exact moment which shows the preservation nature of the AMP. The first order moments clearly coincide with the exact moments. This shows that the AMP holds the mass conservation law.

We have estimated and listed the quantitative errors in the number density functions using relation (21) in Table 1. As expected, errors decrease as the number of terms in the series solution increases. But in HAM and ODM, error increases as the number of terms increases because the series solution diverges for longer time and longer size particles. This demonstrates the higher efficiency and accuracy of the AMP over both HAM and ODM. This shows that the new approach has the tendency to captures the particles in the bigger size domain whereas both HAM and ODM captures particles properties in the shorter size domain only.

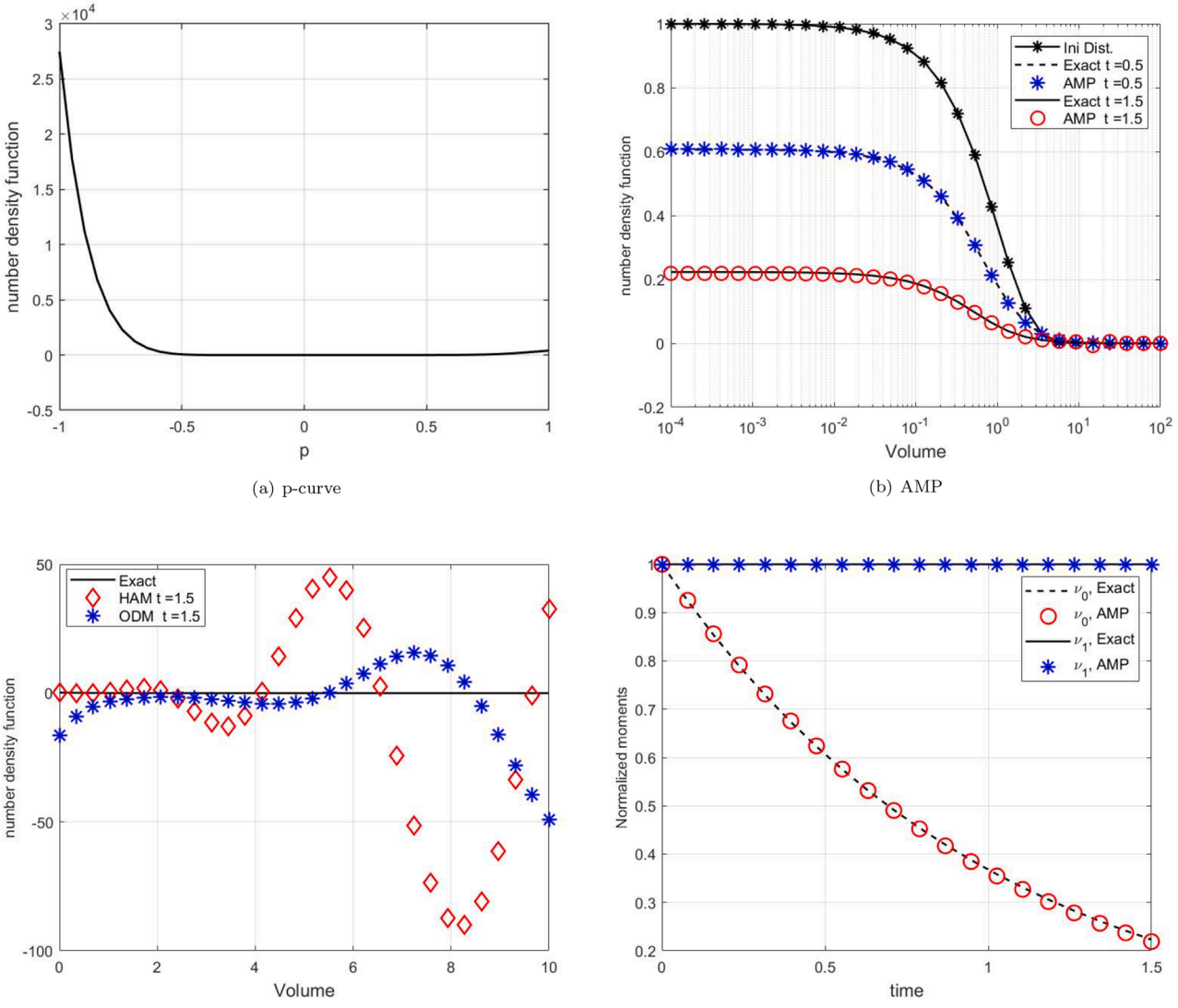
**Table 1**
Error for sum kernel at $t=1.5$ and $y\in[0,10]$ with $\mu_0(y)=e^{-y}$.

| No. of terms (r) | $r=3$ | $r=6$ | $r=9$ |
|---|---|---|---|
| AMP | $17.5922\times10^{-2}$ | $39.4820\times10^{-3}$ | $12.9180\times10^{-3}$ |
| HAM | $34.3322\times10^{-1}$ | $29.6528\times10^{0}$ | $26.6310\times10^{1}$ |
| ODM | $25.0615\times10^{-1}$ | $15.4723\times10^{0}$ | $86.6007\times10^{0}$ |

#### 3.1.2. Polymerization kernel $\alpha(y,w)=(y+c)^{\frac{1}{3}}(w+c)^{\frac{1}{3}}$ with $\mu_0(y)=e^{-y}$ and $\mu_0(y)=4ye^{-2y}$

This kernel has been utilized to model and simulate polymerization problems (Aldous, 1999) arises in chemical engineering. Due to complexity, the analytical solution of (1)-(2) with polymerization kernel does not exist in the literature. Thus, we compare the approximate solution by AMP with finite volume method.

First we consider $c=0$ with Gamma initial distribution $\mu_0(y)=4ye^{-2y}$ and using the iterative formula (12), we get the following




(a) p-curve (b) AMP

(c) HAM and ODM (d) Zeroth and first order Moments

**Fig. 1.** Comparison of number density functions and moments with exact solutions for sum kernel at $t = 0.5$ and $t = 1.5$.

successive iterations for polymerization kernel

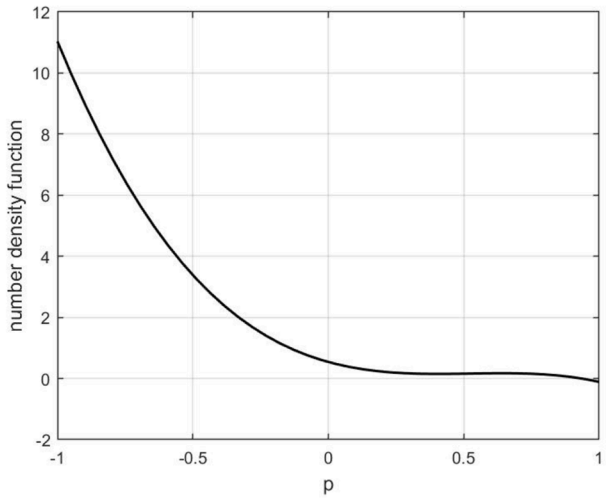
$$\mu_1(t,y,p) = ht\left(\frac{16\sqrt[3]{2}\sqrt{3\pi}e^{-2y}y^{11/3}\Gamma\left(\frac{7}{6}\right)}{55\Gamma\left(\frac{2}{3}\right)} - 2^{5/3}e^{-2y}y^{4/3}\Gamma\left(\frac{7}{3}\right)\right)$$

$$\mu_2(t,y,p) = \frac{h^2e^{-2y}yt^2}{494975180700\Gamma\left(\frac{2}{3}\right)}$$
$$\left(42325920\sqrt{3}\sqrt[3]{y}\left(55\pi\left(27\sqrt[3]{2}\sqrt[3]{y}\Gamma(10/3)+70\Gamma(2/3)\right)\right.\right.$$
$$-1701\sqrt{\pi}\Gamma(7/6)\left(y^{8/3}\Gamma(7/3)+3\sqrt[3]{2}\right)\Big)$$
$$-3808\sqrt[3]{2}\sqrt{3\pi}y^3\left(9509500\sqrt[3]{2}\sqrt{\pi}\Gamma(2/3)\Gamma(4/3)\right.$$
$$\left.-1594323y^{7/3}\Gamma(7/6)\right)\Big)$$
$$+(1-h)ht\left(\frac{16\sqrt[3]{2}\sqrt{3\pi}e^{-2y}y^{11/3}\Gamma\left(\frac{7}{6}\right)}{55\Gamma\left(\frac{2}{3}\right)} - 2^{5/3}e^{-2y}y^{4/3}\Gamma(7/3)\right)$$
$$\vdots$$

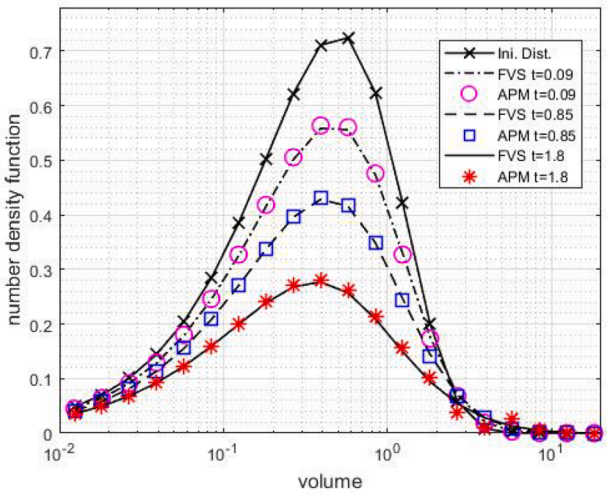
By using the first three iterative terms, the truncated series solution by AMP is given by

$$\vartheta_3(t,y,p) = \frac{989950361400pe^{-2y}t}{494975180700}$$
$$\left(\frac{8\sqrt[3]{2}\sqrt{3\pi}y^{11/3}\Gamma\left(\frac{7}{6}\right)}{55\Gamma\left(\frac{2}{3}\right)} - 2^{2/3}y^{4/3}\Gamma(7/3)\right)+(1-p)$$
$$\left(\frac{8\sqrt[3]{2}\sqrt{3\pi}y^{11/3}\Gamma\left(\frac{7}{6}\right)}{55\Gamma\left(\frac{2}{3}\right)} - 2^{2/3}y^{4/3}\Gamma(7/3)\right)+\ldots$$

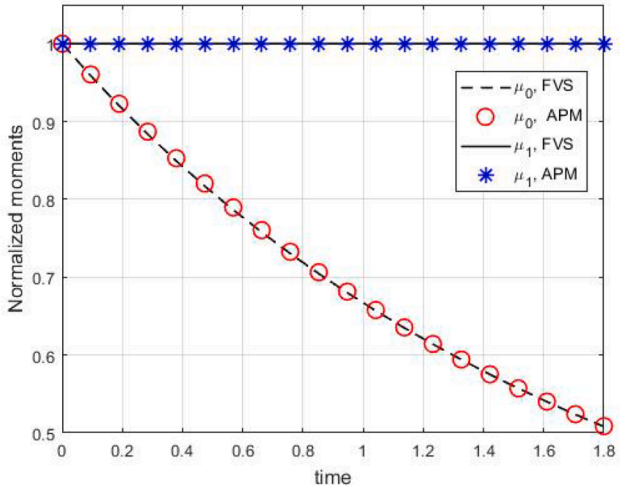
Fig. 2a plots $\vartheta_3(t,y,p)$ against $p$ at $y = 1$ and $t = 2$. The curve seems to be flat in the range $[0.25, 0.8]$. It is within this specific range that the AMP method is expected to achieve rapid convergence. Consequently, the optimal value of $p$ was determined to be 0.65. The AMP solutions of the number density functions are shown in Fig. 2b at different times. We can see that the AMP series solution very high accuracy and matching well with the FVS solution. Moreover, we have plotted zeroth and first order moments in Fig. 2c. It shows that both moments are in good agreement with the FVS solutions.




(a) p-curve




(b) Number density




(c) Moments

**Fig. 2.** Comparison of number density function and moments for polymerization kernel with $\mu_0(y) = 4ye^{-2y}$.

Now we consider $c = 0$ and according to AMP by using iterative formula (12), we get the following successive iterations for polymerization kernel with $\mu_0(y) = e^{-y}$ as follows

$$\mu_1(t,y,p) = pt\left(-\frac{\sqrt[3]{2}\sqrt{3}\pi^{3/2}e^{-y}y^{5/3}}{5\Gamma\left(-\frac{1}{6}\right)\Gamma\left(\frac{2}{3}\right)} - e^{-y}\sqrt[3]{y}\Gamma(4/3)\right)$$

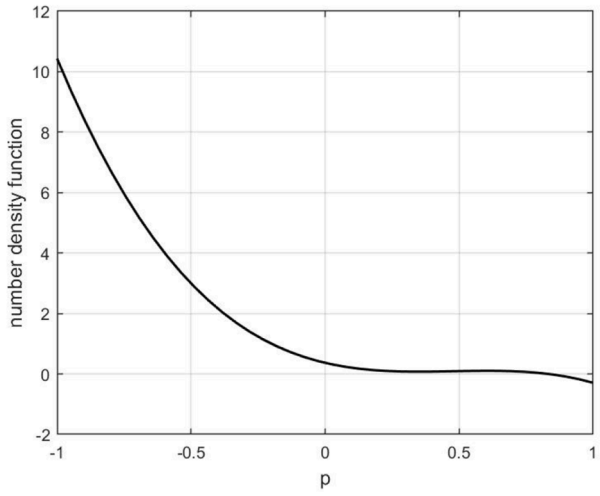
$$\mu_2(t,y,p) = \frac{pe^{-y}\sqrt[3]{yt}}{113400\Gamma\left(-\frac{1}{6}\right)\Gamma\left(\frac{2}{3}\right)}$$
$$\left(\sqrt[3]{2}\pi^{3/2}\sqrt{3}\left(p\left(t\left(-2800y^{5/3}\Gamma(-1/3)\Gamma(2/3) + 11340y^{5/3}\Gamma(4/3)\right.\right.\right.\right.$$
$$\left.\left.\left.\left. - 2187y^3 + 8400\sqrt[3]{y}\Gamma(-1/3) + 22680\right) + 22680y^{4/3}\right) - 22680y^{4/3}\right)$$
$$+ 2800\sqrt[3]{2}\sqrt{\pi}pt\Gamma(-1/3)^3 + 113400$$
$$\left.(p-1)\Gamma(2/3)\Gamma(4/3)\Gamma(-1/6)\right)$$
$$\vdots$$

By using the first three iterative terms, the truncated series solution by AMP is given by

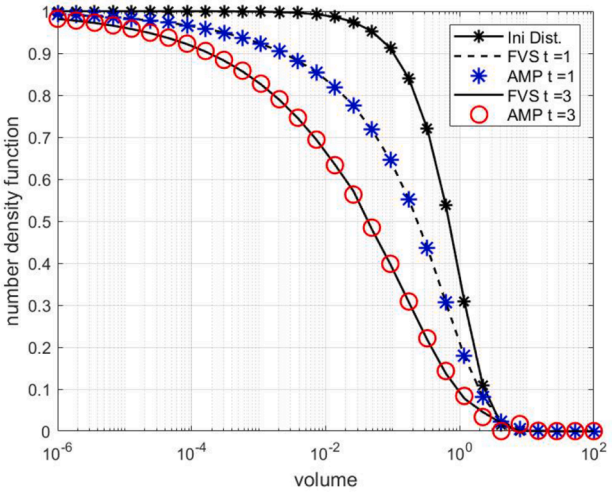
$$\vartheta_3(t,y,p) = e^{-y} + \frac{(p-1)pe^{-y}\sqrt[3]{yt}\left(\sqrt[3]{2}\pi^{3/2}\sqrt{3}(y)^{4/3} + 5\Gamma\left(\frac{2}{3}\right)\Gamma\left(\frac{4}{3}\right)\Gamma\left(-\frac{1}{6}\right)\right)}{5\Gamma\left(-\frac{1}{6}\right)\Gamma\left(\frac{2}{3}\right)}$$
$$- \frac{pe^{-y}\sqrt[3]{yt}\left(\sqrt[3]{2}\pi^{3/2}\sqrt{3}(y)^{4/3} + 5\Gamma\left(\frac{2}{3}\right)\Gamma\left(\frac{4}{3}\right)\Gamma\left(-\frac{1}{6}\right)\right)}{5\Gamma\left(-\frac{1}{6}\right)\Gamma\left(\frac{2}{3}\right)} + \ldots$$

The $p$-curve is plotted against $y = 1$ and $t = 3$ in Fig. 3a for the value of $c = 0$. This plot reveals a horizontally straight region spanning the interval $p \in [0.25, 0.8]$. Within this specific range, the AMP method is anticipated to exhibit efficient convergence. Consequently, the optimal value of $p$ was selected as 0.72 and 0.52 for $t = 1$ and $t = 3$, respectively. After substituting the values of $p$ and $t$, we plotted the AMP solutions in Fig. 3b. We can observe that the number density functions are very well captured by the AMP at times $t = 1$ and $t = 3$, and overlap the FVS solutions.

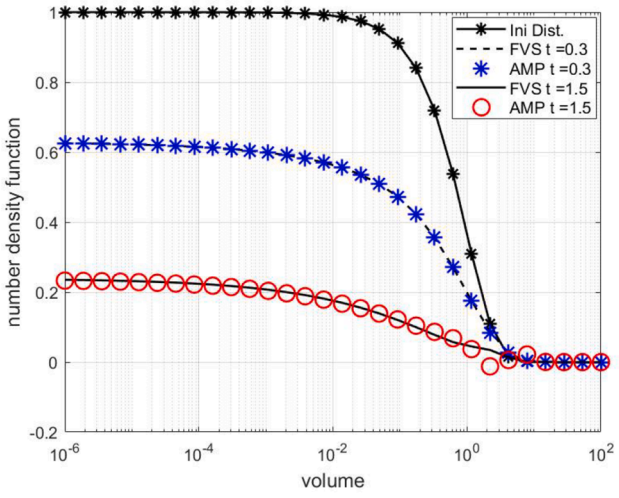
Now, we consider $c = 1$ with exponential initial distribution $\mu_0(y) = e^{-y}$,. According to AMP, by using the iterative formula (12), we get the following successive iterations




(a) p-curve




(b) $c = 0$




(c) $c = 1$

**Fig. 3.** Comparison of number density functions for polymerization kernel with $\mu_0(y) = e^{-y}$.

$$\mu_1(t,y,p) = pt\left(\frac{1}{2}e^{-y}\left(\frac{3y^{4/3}}{2} - \frac{2\sqrt[3]{2}\sqrt{3}\pi^{3/2}y^{5/3}}{5\Gamma\left(-\frac{1}{6}\right)\Gamma\left(\frac{2}{3}\right)} + y\right) - e^{-y}\left(\sqrt[3]{y}+1\right)(1+\Gamma(4/3))\right)$$

$$\mu_2(t,y,p) = \frac{p^2e^{-y}t^2}{720\Gamma\left(-\frac{1}{6}\right)\Gamma\left(\frac{2}{3}\right)}\left(2\left(\sqrt[3]{y}+1\right)\left(5\Gamma(2/3)\Gamma(-1/6)\right.\right.$$
$$\left(-9y^{4/3}(3+\Gamma(1/3)) + 12\sqrt[3]{y}(3+\Gamma(1/3))\right.$$
$$(1+\Gamma(4/3)) - 6y(3+\Gamma(1/3)) + 4\Gamma(1/3)(4+9\Gamma(4/3))$$
$$+ 6(9+12\Gamma(4/3)+\Gamma(2/3)(4\Gamma(4/3)$$
$$\left.-1))\right) + 4\sqrt[3]{2}\pi^{3/2}\sqrt{3}\left(3y^{5/3}(3+\Gamma(1/3)) + 2(9+5\Gamma(2/3))\right)\right)$$
$$+ 9\left(\frac{1}{35}\sqrt[3]{2}(-54)\pi^{3/2}\sqrt{3}y^{10/3} + 20\right.$$
$$y^{4/3}\left(\sqrt[3]{2}\sqrt{\pi}\Gamma(-1/3)^2 - 2\Gamma(-4/3)\Gamma(-1/6)\right)$$
$$+ \frac{8}{27}y^{5/3}\left(27\Gamma(-1/3)\Gamma(-1/6) + 108\sqrt[3]{2}\pi^{3/2}\sqrt{3}\right.$$
$$(1+\Gamma(4/3)) + \sqrt[3]{2}\sqrt{\pi}\left(9\Gamma(-1/3)^2 + 16\Gamma(-4/3)^2\right)\Big)$$
$$+ \frac{260}{21}y^{7/3}\Gamma(-4/3)\Gamma(-1/6) + y^{8/3}\left(-13\sqrt[3]{2}\right.$$
$$\sqrt{3}\pi^{3/2} + 5\Gamma(-4/3)\Gamma(-1/6)\Big) - \frac{8}{729}$$
$$\pi y^3\left(90\sqrt[3]{2}\pi^{3/2} + \sqrt{3}\left(243\sqrt[3]{2}\sqrt{\pi} - 50\Gamma(-4/3)\Gamma(-1/6)\right)\right)$$
$$+ \frac{40}{243}y^2\left(4\sqrt[3]{2}\pi^{3/2}\sqrt{3}\Gamma(-1/3)^2 - 8\sqrt{3}\pi\Gamma(-4/3)\Gamma(-1/6)\right.$$
$$+27\Gamma(-4/3)\Gamma(-1/6)) + \frac{160}{81}y$$
$$\left.\left.\Gamma(-4/3)\left(8\sqrt[3]{2}\sqrt{\pi}\Gamma(-4/3) - 9\Gamma(-1/6)\right)\right)\right) + (1-p)\mu_1(t,y,p)$$

$$\vdots$$

By using the first three iterative terms, the truncated series solution by AMP is given by

$$\vartheta_3(t,y,p) = \frac{1}{720}\left(360pe^{-y}t\left(\frac{3y^{4/3}}{2} - \frac{2\sqrt[3]{2}\sqrt{3}\pi^{3/2}y^{5/3}}{5\Gamma\left(-\frac{1}{6}\right)\Gamma\left(\frac{2}{3}\right)} + y\right.\right.$$
$$\left.\left. - 2\left(\sqrt[3]{y}+1\right)\left(1+\Gamma\left(\frac{4}{3}\right)\right)\right)\right) + 360(1-p)pe^{-y}t + 720e^{-y}\ldots$$

In this particular case, the optimal values of $p$ are 0.72 and 0.32 at $t = 0.3$ and $t = 1.5$, respectively. Fig. 3c shows that the AMP solutions are very well captured and coincide with the FVS solution at $t = 0.3$ and $t = 1.5$. It worth mentioning that the moments results are similar to the one shown for Polymerization kernel with gamma initial distribution. For his reason, the moments solutions for Polymerization kernel with $c = 0$ and $c = 1$ are omitted.

*3.1.3. Ruckenstein/Pulvermacher kernel $\alpha(y,w) = y^{\frac{2}{3}} + w^{\frac{2}{3}}$ with $\mu_0(y) = e^{-y}$ and $\mu_0(y) = 4ye^{-2y}$.*

Again, due to the complexity of Ruckenstein/Pulvermacher kernel, the exact solution of (1)-(2) are not possible. Therefore, we validated the AMP results with FVS. For modeling rennet-induced coagulation and colloidal processes, the Ruckenstein/Pulvermacher kernel has been utilized extensively in the pharmaceutical sciences and dairy industries (Smoluchowski, 1917; McMahon and Brown, 1984).

Now, we evaluate the results for Ruckenstein/Pulvermacher kernel with Gamma initial distribution $\mu_0(y) = 4ye^{-2y}$, from iterative formula (12), we get the following successive iterations:

$$\mu_1(t,y,p) = pt\Big(\frac{18}{11}e^{-2y}y^{11/3} - 2e^{-2y}y\Big(2y^{2/3} + \sqrt[3]{2}\Gamma(8/3)\Big)\Big)$$

$$\begin{aligned}\mu_2(t,y,p) = p\Big(&2pe^{-2y}y^{7/3}t^2 - \frac{981}{715}pe^{-2y}y^{13/3}t^2 + \frac{81}{836}pe^{-2y}y^{19/3}t^2\\ &+ \frac{9pe^{-2y}y^{5/3}t^2\Gamma\left(\frac{11}{3}\right)}{4\,2^{2/3}} - \frac{9}{11}\sqrt[3]{2}p\\ &e^{-2y}y^{11/3}t^2\Gamma\Big(\frac{8}{3}\Big) - \frac{27pe^{-2y}y^{11/3}t^2\Gamma\left(\frac{11}{3}\right)}{88\,2^{2/3}}\\ &+ 2^{2/3}he^{-2y}yt^2\Gamma(8/3)^2 - \frac{21pe^{-2y}yt^2\Gamma\left(\frac{10}{3}\right)}{44\sqrt[3]{2}}\\ &+ \frac{135\pi\sqrt{3}pe^{-2y}y^{19/3}t^2\Gamma\left(\frac{5}{3}\right)}{1729\Gamma\left(\frac{1}{3}\right)^2} - \frac{60\sqrt{3}\pi pe^{-2y}y^{13/3}t^2\Gamma\left(\frac{5}{3}\right)}{91\Gamma\left(\frac{1}{3}\right)^2}\Big)\\ &+ (1-p)\mu_1(t,y,p)\\ &\vdots\end{aligned}$$

By using the first five iterative terms, the truncated series solution by AMP is given by

$$\begin{aligned}\vartheta_5(t,y,p) =& e^{-2y}y\big(8702\pi pt\Gamma(-2/3)\Gamma(-5/3)\Gamma(-8/3)\Gamma(-5/6)\\ &+ 382\pi\Gamma(2/3)\Gamma(4/3)\Gamma(5/3)\Gamma(-1/3)\\ &\Gamma(-2/3)\Gamma(-5/3)\Gamma(-8/3)\Gamma(1/6)^3\Gamma(-5/6) + \ldots\end{aligned}$$

For $y = 10$ and $t = 3$, we draw the $p$-curve for the various $p$ values. Fig. 4a demonstrates that the $p$-curve plot is straight in the range $[-0.4, 0.6]$. As a result, the AMP solution will converge during this time interval. For this case, the optimal value of $p = .53$ at $t = 0.05, 0.47, 1$ respectively. We obtain the series solution of AMP by substituting the value of $p$ at different values of time (see Fig. 4). Fig. 4b shows that AMP and FVS results are in a good agreement till $t = 1$ for the Ruckenstein kernel with Gamma initial distribution. Furthermore, both zeroth and first order moments by AMP and FVS are plotted in Fig. 4c and AMP results clearly overlap with FVS.

Here for Ruckenstein/Pulvermacher kernel with $\mu_0(y) = e^{-y}$, using the iterative formula (12), we get the following successive iterations

$$\mu_1(t,y,p) = pt\Big(\frac{3}{5}e^{-y}y^{5/3} - e^{-y}\big(y^{2/3} + \Gamma(5/3)\big)\Big)$$

$$\begin{aligned}\mu_2(t,y,p) = p\Big(&\frac{1}{2}pe^{-y}y^{4/3}t^2 - \frac{18}{35}pe^{-y}y^{7/3}t^2 + \frac{9}{100}pe^{-y}y^{10/3}t^2\\ &+ \frac{3}{2}pe^{-y}y^{2/3}t^2\Gamma(5/3) - \frac{9}{10}pe^{-y}y^{5/3}\\ &t^2\Gamma(5/3) - \frac{3\sqrt{\pi}pe^{-y}y^{7/3}t^2\Gamma\left(\frac{8}{3}\right)}{40\sqrt[3]{2}\Gamma\left(\frac{13}{6}\right)} + \frac{9\sqrt{\pi}pe^{-y}y^{10/3}t^2\Gamma\left(\frac{8}{3}\right)}{400\sqrt[3]{2}\Gamma\left(\frac{13}{6}\right)}\\ &+ pe^{-y}t^2\Gamma(5/3)^2 - \frac{1}{5}pe^{-y}t^2\Gamma(7/3)\Big)\\ &+ (1-p)pt\Big(\frac{3}{5}e^{-y}y^{5/3} - e^{-y}\big(y^{2/3} + \Gamma(5/3)\big)\Big)\\ &\vdots\end{aligned}$$

By using the first five iterative terms, the truncated series solution by AMP is given by

$$\begin{aligned}\vartheta_3(t,y,p) =& e^{-y}\big(1 + pt\big(-5y^{2/3} + 3y^{5/3} - 5\Gamma(5/3)\big)\\ &+ \big(p^2t\big(-725760\sqrt{3}\pi^{3/2}y^{5/3}t\Gamma(-2/3)\Gamma(1/6)\\ &\Gamma(7/6)\Gamma(13/6) + 802^{2/3}\sqrt{3}\pi^2t\ldots\end{aligned}$$

Now we compare the results of the number density function obtained for the Ruckenstein/Pulvermacher kernel with $e^{-y}$ in Fig. 5). In this instance, we plot the $p$-curve corresponding to the optimal value of $p$ for $y = 1$ and $t = 1.5$, as shown in Fig. 5a. The curve remains straight over the interval $[0, 1]$. Consequently, the convergence control parameter is chosen as 0.72 for $t = 0.5$ and 0.55 for $t = 1.5$, respectively. The qualitative results of the number density functions predicted by the AMP and FVS are plotted in Fig. 5b. It demonstrates that AMP and FVS results coincide for all times which shows the applicability of AMP method to capture the number density functions for shorter and longer time domains.

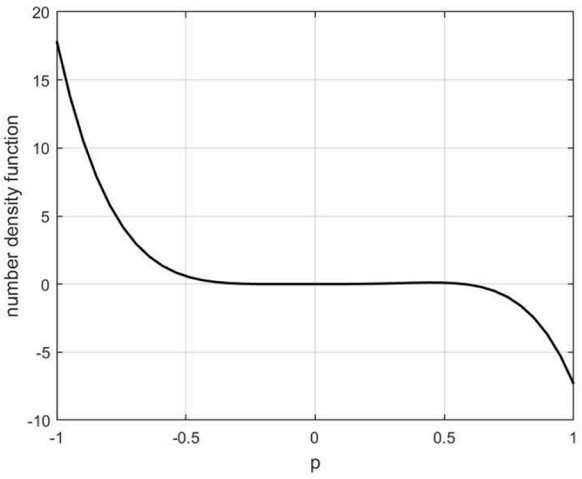
*3.1.4. Shear kernel $\alpha(y,w) = \left(y^{\frac{1}{3}} + w^{\frac{1}{3}}\right)^3$ with $\mu_0(y) = e^{-y}$ and $\mu_0(y) = 4ye^{-2y}$.*

For shear kernel, the analytical solution of (1)-(2) are very challenging to obtain. This kernel has been used to develop the models of sprayed fluidized granulator models (Hussain et al., 2014).

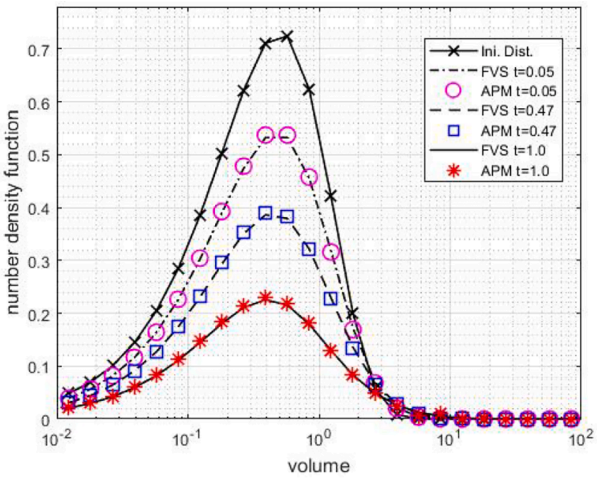
Now we take shear kernel with Gamma initial distribution $\mu_0(y) = 4ye^{-2y}$, and from iterative formula (12), we get the following successive iterations:

$$\begin{aligned}\mu_1(t,y,p) =& pe^{-2y}t\Big(\frac{4}{243}y^4\Big(40\pi\sqrt{3} + 81\Big) - 2y\big(4\,2^{2/3}y^{2/3}\Gamma(4/3)\\ &+2y + 3\sqrt[3]{2}\sqrt[3]{y}\Gamma(8/3) + 2\big)\Big)\end{aligned}$$

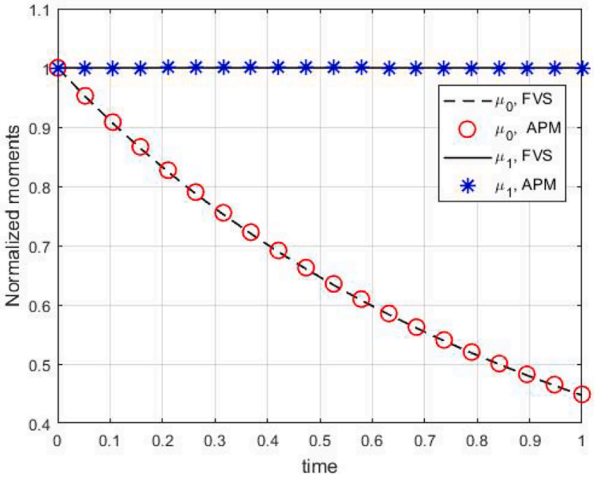
$$\begin{aligned}\mu_2(t,y,p) =& pe^{-2y}\Big(-\frac{20\sqrt[3]{2}py^{13/3}\pi t^2\Gamma\left(\frac{8}{3}\right)}{27\sqrt{3}} - \frac{40py^4\pi t^2}{81\sqrt{3}} - \frac{40py^5\pi t^2}{81\sqrt{3}}\\ &- \frac{40py^4\pi t^2}{81\sqrt{3}} - \frac{40py^5\pi t^2}{81\sqrt{3}} - \frac{80\,2^{2/3}py^{14/3}\pi t^2\Gamma\left(\frac{4}{3}\right)}{81\sqrt{3}} + \frac{4}{45}py^7t^2\\ &- \frac{4}{3}py^5t^2 - 2py^4t^2 + 2py^3t^2 + \frac{10880py^7\pi^2t^2}{177147}\\ &+ 6py^2t^2 + 2pyt^2 + \frac{1}{3}\sqrt[3]{256}py^{4/3}t^2\Gamma(4/3)^2\\ &+ 16\sqrt[3]{2}py^{7/3}t^2\Gamma(4/3)^2 + 9\,2^{2/3}py^{5/3}t^2\\ &\Gamma(8/3)^2 - \frac{96}{55}\sqrt[3]{2}\sqrt{3}py^{14/3}t^2\Gamma(7/6)^2\\ &+ \frac{1}{81}2^{2/3}1867py^{5/3}t^2\Gamma(4/3) + 8\,2^{2/3}py^{8/3}t^2\Gamma(4/3)\\ &- \frac{1172}{231}2^{2/3}py^{14/3}t^2\Gamma(4/3) + \frac{1}{27}\sqrt[3]{2440}py^{4/3}t^2\Gamma(8/3)\\ &+ 6\sqrt[3]{2}py^{7/3}t^2\Gamma(8/3) - \sqrt[3]{2}py^{13/3}t^2\\ &\Gamma(8/3) - \frac{120}{91}2^{2/3}\sqrt{3}py^{13/3}t^2\Gamma(5/6)\Gamma(11/6)\\ &- \frac{20\sqrt[3]{2}y^{13/3}p\pi t^2\Gamma\left(\frac{8}{3}\right)}{27\sqrt{3}} - \frac{80\,2^{2/3}p\pi y^{14/3}t^2\Gamma\left(\frac{4}{3}\right)}{81\sqrt{3}}\\ &- \frac{248\sqrt[3]{2}py^{13/3}\pi t^2}{91\sqrt{3}\Gamma\left(\frac{4}{3}\right)} + \frac{560py^2\pi t^2}{27\sqrt{3}} - \frac{80py^5\pi t^2}{81\sqrt{3}} - \frac{160py^4\pi t^2}{81\sqrt{3}}\end{aligned}$$




(a) p-curve with $4ye^{-2y}$

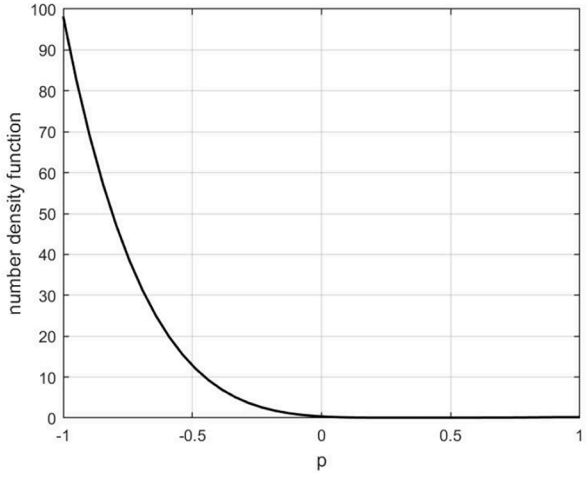



(b) Number density with $4ye^{-2y}$

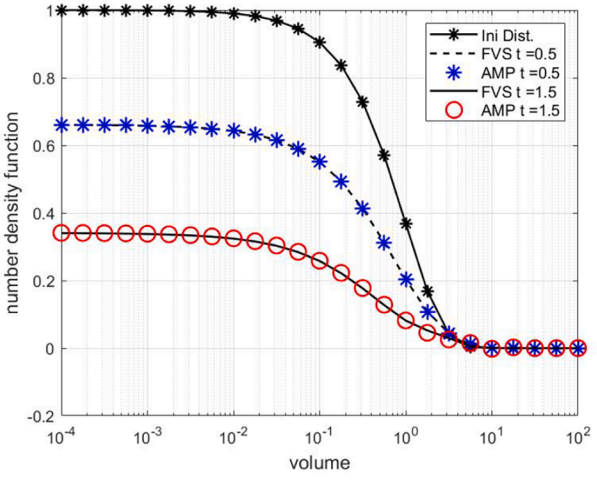



(c) Moments with gamma initial distribution

**Fig. 4.** Comparison of Number density function and moments for Ruckenstein/Pulvermacher kernel with $4ye^{-2y}$.




(a) p-curve with $e^{-y}$




(b) Number density with $e^{-y}$

**Fig. 5.** Comparison of Number density function and moments for Ruckenstein/Pulvermacher kernel with $e^{-y}$.

$$-\frac{6160\sqrt[3]{2}py^{4/3}\pi t^2\Gamma\left(\frac{8}{3}\right)}{729\sqrt{3}}+\frac{560py^7\pi t^2}{2187\sqrt{3}}-\frac{18200\,2^{2/3}py^{5/3}\pi t^2\Gamma\left(\frac{4}{3}\right)}{2187\sqrt{3}}\Bigg)+(1-p)\mu_1(t,y,p)$$
$$\vdots$$

By using the first three iterative terms, the truncated series solution by AMP is given by

$$\begin{aligned}\vartheta_3(t,y,p)=&e^{-2y}\Bigg(\frac{40\pi p^3y^6t^3}{243\sqrt{3}}+\frac{2}{729}\left(80\pi\sqrt{3}+243\right)p^3y^6t^3\\&-\frac{4\left(18900\pi\sqrt{3}+13600\pi^2+19683\right)p^3y^8t^3}{885735}\\&-\frac{2}{3}y\left(p^3t\left(t^2+6t+6\right)-9p^2t(t+2)+18pt-6\right)+\ldots\end{aligned}$$

For the different values of $p$, we plotted the $p$-curve for $y=1$ and $t=0.2$. As shown in Fig. 6a, the $p$-curve plot is straight in the interval $[0.25,0.8]$. Thus, the AMP solution will converge in this interval. For this particular case, the optimal value of $p$ is chosen 0.68 at $t=0.009$, 0.08, and 0.18, respectively. The comparison of the number density functions obtained by AMP and FVS for the shear kernel with Gamma initial distribution is shown in Fig. 6b. It can be noted that the AMP solutions match well with the FVS solutions. Fig. 6e shows that both zeroth and first order moment exactly match with FVS.

Now we consider shear kernel with $\mu_0(y)=e^{-y}$, and using iterative formula (12), we get the following successive iterations

$$\begin{aligned}\mu_1(t,y,p)=&pt\Big(\frac{1}{18}e^{-y}y^2\left(4\pi\sqrt{3}+9\right)\\&-e^{-y}\left(y^{2/3}\Gamma(1/3)+y+3\sqrt[3]{y}\Gamma(5/3)+1\right)\Big)\\\mu_2(t,y,p)=&(1-p)\mu_1(t,y,p)+p\Bigg(-\frac{e^{-y}py^{7/3}\pi t^2\Gamma\left(\frac{5}{3}\right)}{2\sqrt{3}}-\frac{e^{-y}py^2\pi t^2}{6\sqrt{3}}\\&-\frac{e^{-y}py^3\pi t^2}{6\sqrt{3}}-\frac{e^{-y}py^2\pi t^2}{6\sqrt{3}}\\&-\frac{e^{-y}py^3\pi t^2}{6\sqrt{3}}-\frac{e^{-y}py^{8/3}\pi t^2\Gamma\left(\frac{1}{3}\right)}{6\sqrt{3}}+\frac{1}{12}e^{-y}py^4t^2-\frac{1}{2}e^{-y}py^3t^2\\&+\frac{34}{729}e^{-y}py^4\pi^2t^2-\frac{1}{4}e^{-y}py^2t^2+\frac{1}{2}e^{-y}pt^2+\frac{3}{2}e^{-y}pyt^2\\&+\frac{2}{3}e^{-y}p\sqrt[3]{y}t^2\Gamma\left(\frac{1}{3}\right)^2+\frac{1}{2}e^{-y}py^{4/3}t^2\Gamma(1/3)^2\\&+9e^{-y}py^{2/3}t^2\Gamma(5/3)^2+\frac{26}{9}e^{-y}py^{2/3}t^2\Gamma(1/3)\\&+e^{-y}py^{5/3}t^2\Gamma(1/3)-\frac{1}{4}e^{-y}py^{8/3}t^2\Gamma(1/3)\\&+\frac{49}{6}e^{-y}p\sqrt[3]{y}t^2\Gamma(5/3)+3e^{-y}py^{4/3}t^2\Gamma(5/3)\\&-\frac{291}{112}e^{-y}py^{7/3}t^2\Gamma(5/3)-\frac{e^{-y}py^{7/3}\pi t^2\Gamma\left(\frac{5}{3}\right)}{2\sqrt{3}}\\&-\frac{e^{-y}h\pi t^2y^{8/3}\Gamma\left(\frac{1}{3}\right)}{6\sqrt{3}}-\frac{9\sqrt{3}e^{-y}pm^{7/3}\pi t^2}{28\Gamma\left(\frac{1}{3}\right)}\\&-\frac{e^{-y}py^{8/3}t^2\Gamma\left(\frac{1}{3}\right)^3}{12\Gamma\left(\frac{8}{3}\right)}-\frac{17e^{-y}py^{8/3}\pi t^2}{12\sqrt{3}\Gamma\left(\frac{8}{3}\right)}\\&-\frac{9e^{-y}py^{7/3}\sqrt{\pi}t^2\Gamma\left(\frac{5}{3}\right)^2}{8\sqrt[3]{2}\Gamma\left(\frac{13}{6}\right)}-\frac{e^{-y}py^3\pi t^2}{3\sqrt{3}}\\&-\frac{2e^{-y}py^2\pi t^2}{3\sqrt{3}}+\frac{14e^{-y}py\pi t^2}{3\sqrt{3}}-\frac{40e^{-y}p\sqrt[3]{y}\pi t^2\Gamma\left(\frac{5}{3}\right)}{9\sqrt{3}}\\&-\frac{28e^{-y}py^{2/3}\pi t^2\Gamma\left(\frac{1}{3}\right)}{27\sqrt{3}}+\frac{35e^{-y}py^4\pi t^2}{162\sqrt{3}}\Bigg)\\&\vdots\end{aligned}$$

By using the first three iterative terms, the truncated series solution by AMP is given by

$$\begin{aligned}\vartheta_3(t,y,p)=&\Big(e^{-y}\big(160868466158400\Gamma(1/6)\Gamma(1/3)^2\Gamma(5/6)\Gamma(5/3)^2\\&\Gamma(13/6)\Gamma(8/3)\Gamma(11/3)\\&-26811411026400pt\Gamma(1/6)\Gamma(1/3)^2\Gamma(5/6)\ldots\end{aligned}\tag{24}$$

After obtaining the TSS (24), we plot the $p$-curve at $y=1$ and $t=0.5$, which predicts a straight line for $p$ in the range $[0.1,0.75]$ as shown in Fig. 6c. In this case, the optimal values of $p$ are 0.72 and 0.52 at $t=0.2$ and $t=0.5$, respectively. The series solution of AMP by substituting the values of $p$ and $t$ has been plotted in Fig. 6d. It shows AMP agrees with FVS and offers excellent solutions for the number density functions.

### 3.2. Testing for 2D aggregation equation

The applicability of the proposed methodology is further substantiated by its extension to approximate the solution of 2D aggregation equation. The 2D aggregation model holds significant relevance across various domains, particularly within pharmaceutical sciences where it underpins processes critical to granule formulation, including sprayed fluidized bed granulation and twin-screw granulation (Chaudhury et al., 2013; Shirazian et al., 2019). Arora et al. (2024) applied the homotopy perturbation method (HPM) to derive semi-analytical solutions for both $1D$ and $2D$ nonlinear aggregation equations. However, the results demonstrated for the $2D$ HPM application are notably limited as they presented results for short time (specifically at $t=1$) and are restricted to the size independent constant kernel.

#### 3.2.1. Constant kernel $\alpha(y,w,z,x)=1$ with initial condition

$\mu_0(y,z)=\frac{4N_0}{y_0z_0}\left(\frac{y}{y_0}\right)e^{\left(-\frac{2y}{y_0}-\frac{z}{z_0}\right)}$

The exact solution is given (Gelbard and Seinfeld, 1978; Qamar and Warnecke, 2007) as

$$\mu(t,y,z)=\frac{16N_0}{y_0z_0(\tau+2)^2}e^{\left(-\frac{2y}{y_0}-\frac{z}{z_0}\right)}\sum_{k=0}^{\infty}\frac{\left(\frac{4\tau z}{(\tau+2)z_0}\right)^k\left(\frac{y}{y_0}\right)^{2k+1}}{k!\,(2k+1)!}.\tag{25}$$

Here $\tau=b_0N_0t$ is the dimensionless time. The following expressions represent the exact moments of the aggregation equation corresponding to the specified kernel and initial condition (Qamar and Warnecke, 2007):

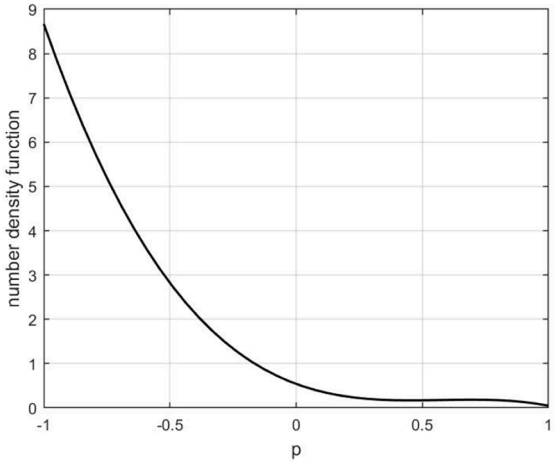
$$\nu_{(0,0)}(\tau)=\frac{2N_0}{2+\tau},\nu_{10}(\tau)+\nu_{01}(\tau)=\text{Constant, and}\nu_{(1,1)}(\tau)=y_0z_0N_0(1+\tau).\tag{26}$$

For numerical computations, we choose $N_0=1$ , $b_0=1$, $y_0=1$ and $z_0=1$. Then, using recursive scheme (18), we get

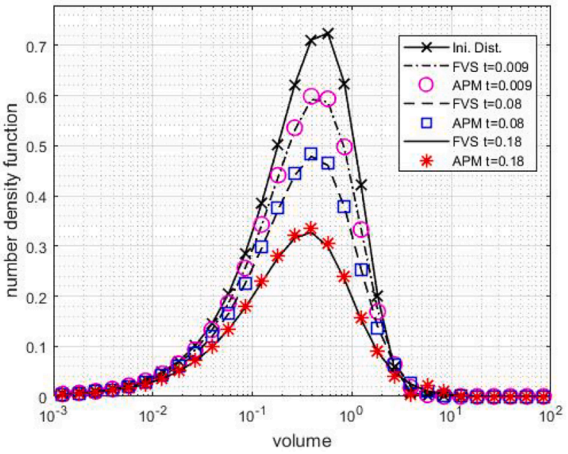
$$\begin{aligned}\mu_0(t,y,z)&=4\,y\,\mathrm{e}^{-2\,y-z},\\\mu_1(t,y,z,p)&=\frac{4\,p\,t\,y\,\mathrm{e}^{-2\,y-z}\left(y^2\,z-3\right)}{3},\\\mu_2(t,y,z,p)&=\frac{p^2\,t^2\,y\,\mathrm{e}^{-2\,y-z}\left(y^4\,z^2-30\,y^2\,z+45\right)}{15}\\&\quad-\frac{4\,p\,t\,y\,\mathrm{e}^{-2\,y-z}\left(y^2\,z-3\right)(p-1)}{3},\end{aligned}\tag{27}$$

and so on. Due to the complexity of the higher order terms, a 8-terms TSS for the number density function is given as below

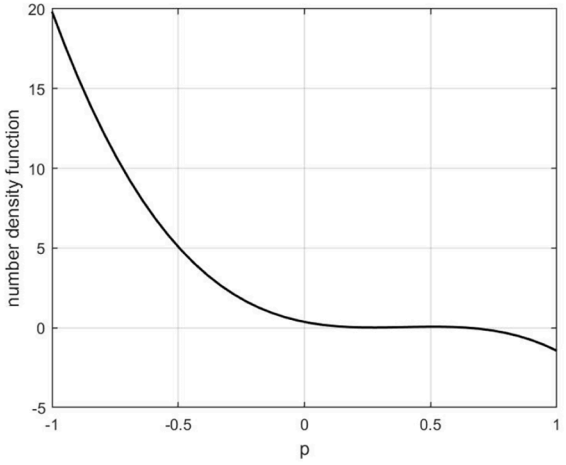
$$\vartheta_8(t,y,z,p)=4\,y\,\mathrm{e}^{-2\,y-z}+\frac{4\,p\,t\,y\,\mathrm{e}^{-2\,y-z}\left(y^2\,z-3\right)}{3}$$



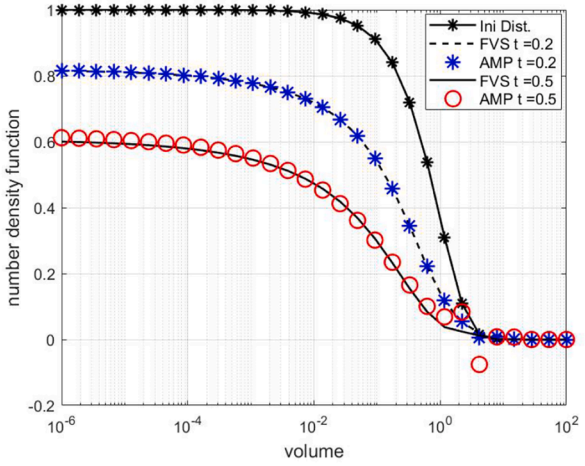

(a) p-curve



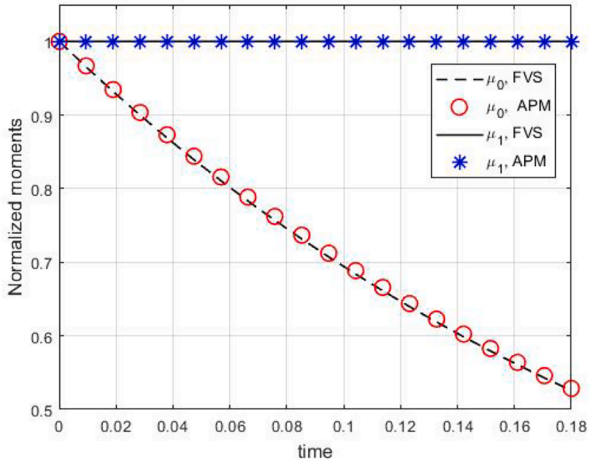

(b) Number density with gamma initial distribution




(c) p-curve

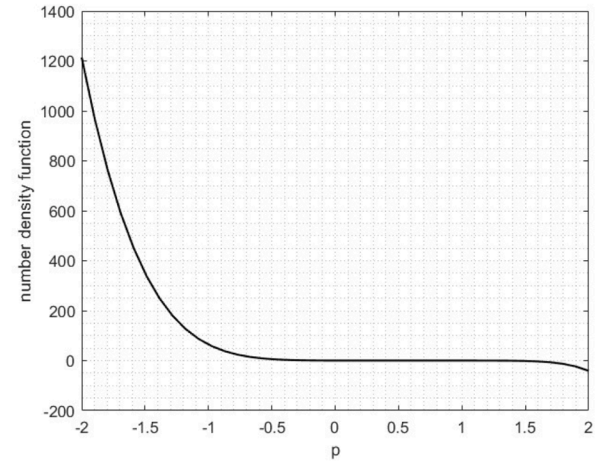



(d) Number density with exponential initial distribution

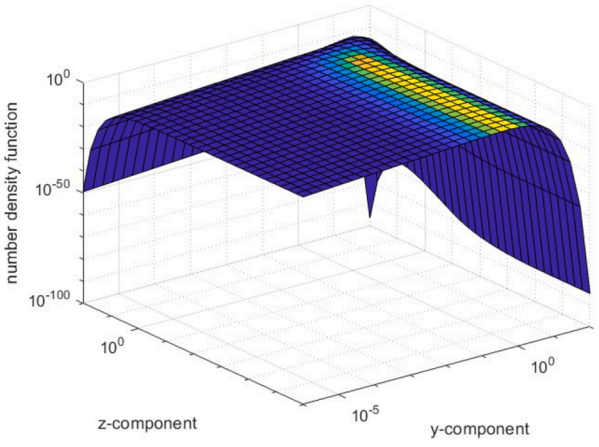



(e) Moments with gamma initial distribution

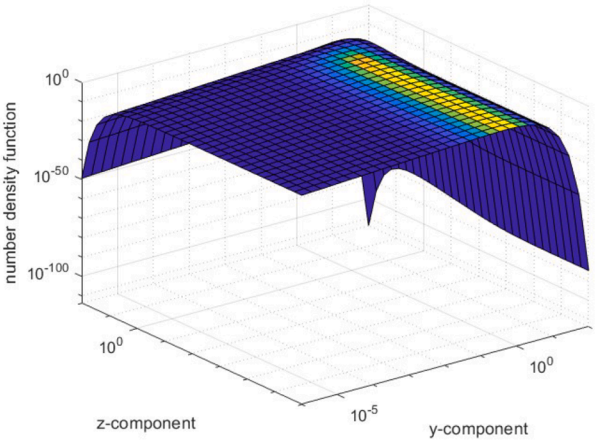
**Fig. 6.** Comparison of Number density function and moments for Shear kernel by AMP and FVS solution.



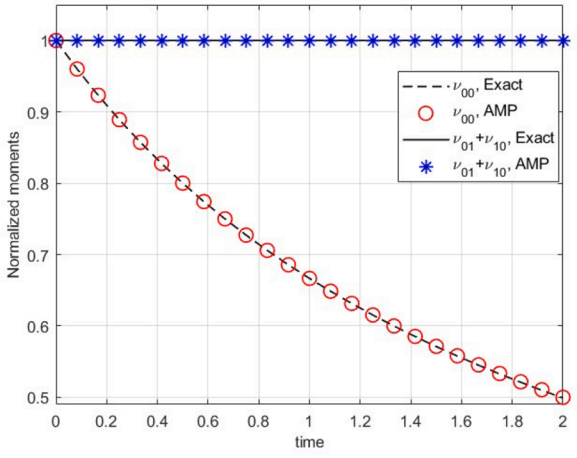

(a) p-curve




(b) Number density functions with AMP




(c) Number density functions with Exact solution

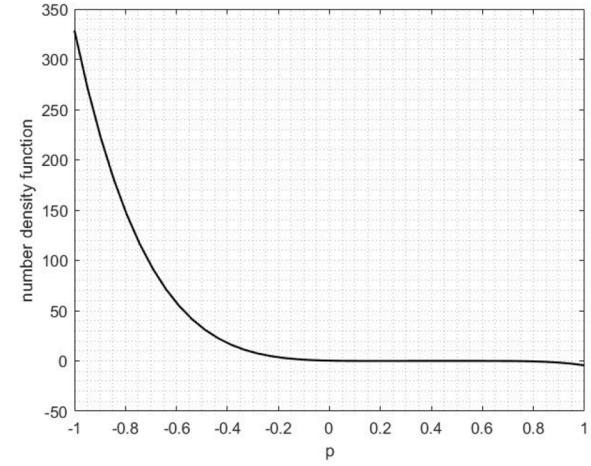



(d) Zeroth and first order moments

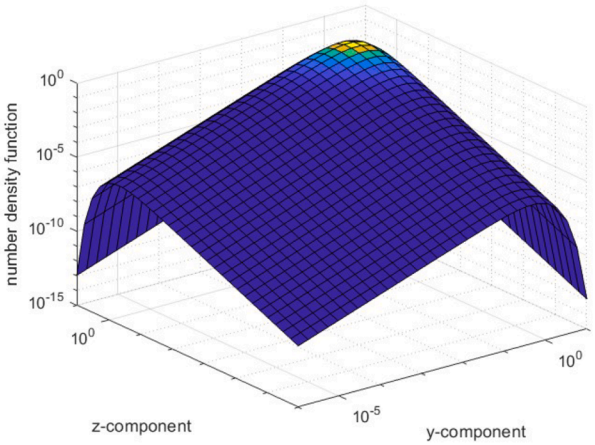
**Fig. 7.** Comparison of AMP and Exact solution for constant kernel with exponential initial distribution $\mu_0(t, y, z) = 4ye^{-2y-z}$.

$$+\frac{p^2 t^2 y\, e^{-2y-z}\left(y^4 z^2 - 30 y^2 z + 45\right)}{15} - \frac{4 p t y\, e^{-2y-z}\left(y^2 z - 3\right)(p-1)}{3} + \ldots \tag{28}$$

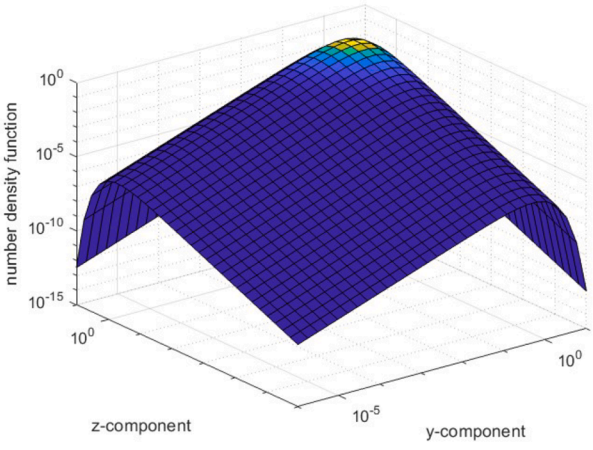
Now, the optimal range for the convergence control parameter $p$ is determined by examining the $p$-curve for the $\vartheta_8$ component (Fig. 7a), plotted at $y = 1$, $z = 1$, and $t = 1$. The curve exhibits a flat region spanning the interval $p \in [-0.5, 1.70]$. Consequently, the AMP method is antici-



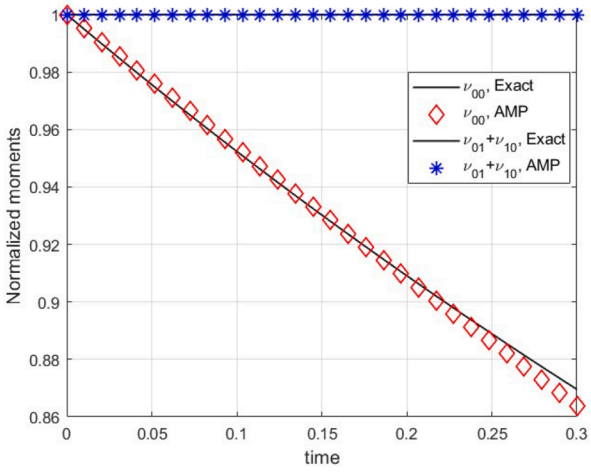

(a) p-curve




(b) Number density functions with AMP

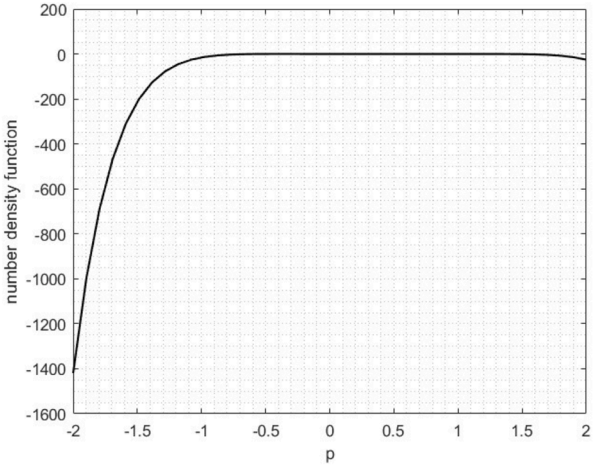



(c) Number density functions with Exact solution

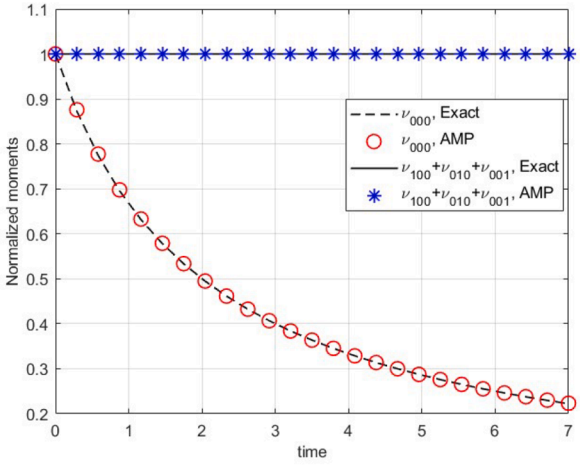



(d) Zeroth and first order moments

**Fig. 8.** Comparison of AMP and Exact solution for sum kernel with exponential initial distribution $\mu_0(t, y, z) = 16yze^{-2y-2z}$.




(a) p-curve




(b) Zeroth and first order moments

**Fig. 9.** Comparison of AMP and Exact solution for constant kernel with exponential initial distribution $\mu_0(t, y, z) = e^{(-y-z-q)}$.

pated to converge efficiently within this interval. Specifically, the optimal value of $p$ is selected as 0.5. The series solutions obtained by substituting this values of $p$ into (28) are compared with the exact solution given in (25), as shown in Figs. 7b and 7c. To further assess the accuracy of the method, we evaluate the zeroth-order moment $\nu_{00}$, which quantifies the total number of particles, and the first order moment $(\nu_{01}+\nu_{10})$, which represents the total volume of the particles. The close agreement between the computed and exact moments, as shown in Fig. 7d, demonstrates the reliability and effectiveness of the proposed approach.

*3.2.2. Sum kernel $\alpha(y,w,z,x)=y+w+z+x$ with initial condition $\mu_0(y,z)=\frac{16N_0yz}{y_0^2z_0^2}e^{\left(-\frac{2y}{y_0}-\frac{2z}{z_0}\right)}$.*

The analytical solution as reported in Fernandez-Diaz and Gomez-Garcia (2007), is formulated as:

$$\zeta(t,y,z)=N_0(1-\tau)e^{\left(\frac{-(y+z)\tau}{y_0+z_0}\right)}\left[\frac{(\rho_1+1)(\rho_2+1)}{y_0z_0}\right]e^{\left(-\frac{(\rho_1+1)y}{y_0}-\frac{(\rho_2+1)z}{z_0}\right)} \times\sum_{k=0}^{\infty}\frac{\frac{1}{(k+1)!}\left(\frac{(y+z)\tau}{y_0+z_0}\right)^k\left[(\rho_1+1)^{(k+1)(\rho_1+1)-1}(\rho_2+1)^{(k+1)(\rho_2+1)-1}\left(\frac{y}{y_0}\right)^{(k+1)(\rho_1+1)-1}\left(\frac{z}{z_0}\right)^{(k+1)(\rho_2+1)-1}\right]}{\Gamma\big((\rho_1+1)(k+1)\big)\Gamma\big((\rho_2+1)(k+1)\big)}. \tag{29}$$

where, $\tau=1-e^{(\alpha_1\phi t)}$, $\alpha_0$ is a constant and $\phi$ is the total mass of the particles in the system. For numerical computations, we choose $N_0=1$ , $\alpha_0=1$ , $\rho_1=1$ , $\rho_2=1$, $y_0=1$ and $z_0=1$. Using recursive scheme (18), we get

$$\begin{aligned}
\mu_0(t,y,z)&=16\,y\,z\,e^{-2y-2z},\\
\mu_1(t,y,z,p)&=-\frac{16\,p\,t\,y\,z\,e^{-2y-2z}\left(-2y^3z^2-2y^2z^3+9y+9z+18\right)}{9},\\
\mu_2(t,y,z,p)=&\,p\Bigg(32\,p\,y\,z\,e^{-2y-2z}+48\,p\,y\,z^2\,e^{-2y-2z}+48\,p\,y^2\,z\,e^{-2y-2z}\\
&+8\,p\,y\,z^3\,e^{-2y-2z}+8\,p\,y^3\,z\,e^{-2y-2z}\\
&+16\,p\,y^2\,z^2\,e^{-2y-2z}-\frac{32\,p\,y^3\,z^4\,e^{-2y-2z}}{3}\\
&-\frac{32\,p\,y^4\,z^3\,e^{-2y-2z}}{3}-\frac{32\,p\,y^3\,z^5\,e^{-2y-2z}}{9}\\
&-\frac{64\,p\,y^4\,z^4\,e^{-2y-2z}}{9}\\
&-\frac{32\,p\,y^5\,z^3\,e^{-2y-2z}}{9}+\frac{32\,p\,y^5\,z^7\,e^{-2y-2z}}{675}+\frac{64\,p\,y^6\,z^6\,e^{-2y-2z}}{675}\\
&+\frac{32\,p\,y^7\,z^5\,e^{-2y-2z}}{675}\Bigg)t^2\\
&+\frac{16\,p\,y\,z\,e^{-2y-2z}\,(p-1)\left(-2y^3z^2-2y^2z^3+9y+9z+18\right)t}{9},
\end{aligned} \tag{30}$$

and so on. Due to the intricate nature of the higher-order terms, a 5-term TSS for the number density function is presented as follows

$$\begin{aligned}
\vartheta_5(t,y,z,p)=&16\,y\,z\,e^{-2y-2z}\\
&-\frac{16\,p\,t\,y\,z\,e^{-2y-2z}\left(-2y^3z^2-2y^2z^3+9y+9z+18\right)}{9}\\
&+p\Bigg(32\,p\,y\,z\,e^{-2y-2z}+48\,p\,y\,z^2\,e^{-2y-2z}+48\,p\,y^2\,z\,e^{-2y-2z}\\
&+8\,p\,y\,z^3\,e^{-2y-2z}+8\,p\,y^3\,z\,e^{-2y-2z}\\
&+16\,p\,y^2\,z^2\,e^{-2y-2z}-\frac{32\,p\,y^3\,z^4\,e^{-2y-2z}}{3}\\
&-\frac{32\,p\,y^4\,z^3\,e^{-2y-2z}}{3}-\frac{32\,p\,y^3\,z^5\,e^{-2y-2z}}{9}\\
&-\frac{64\,p\,y^4\,z^4\,e^{-2y-2z}}{9}-\frac{32\,p\,y^5\,z^3\,e^{-2y-2z}}{9}\\
&+\frac{32\,p\,y^5\,z^7\,e^{-2y-2z}}{675}+\frac{64\,p\,y^6\,z^6\,e^{-2y-2z}}{675}\\
&+\frac{32\,p\,y^7\,z^5\,e^{-2y-2z}}{675}\Bigg)t^2\\
&+\frac{16\,p\,y\,z\,e^{-2y-2z}\,(p-1)\left(-2y^3z^2-2y^2z^3+9y+9z+18\right)t}{9}\\
&+\ldots
\end{aligned} \tag{31}$$

Fig. 8a provides the TSS (31) against $p$ at $y=1$, $z=1$, $t=1$ and shows that $p$-curve remains flat between $[-0.15, 0.9]$. When $p$ is selected from this specified range, the method is expected to exhibit efficient and faster convergence. The truncated series solution (31) of the AMP method , evaluated at $p=.052$, is compared against the exact number density function, with the resulting three-dimensional plots for AMP and the exact solution presented in Figures 8b and 8c, respectively. Furthermore, Figure 8d presents a comparative illustration of the zeroth and first-order moments obtained via the AMP method against the exact solutions. It can be easily observed that the AMP results demonstrate excellent agreement with the exact solutions.

### *3.3. Testing for 3D aggregation equation with constant kernel $\alpha(y,w,z,x,q,s)=1$ with initial condition $\mu_0(y,z,q)=e^{(-y-z-q)}$*

Now, we implement the AMP method to solve the nonlinear three-dimensional aggregation equation in which each particle has three intrinsic properties. To the best of our knowledge, no semi-analytical approach is available for solving a three-dimensional nonlinear aggregation equation.

Fig. 9a shows the plot of the $p$-curve, which remains nearly horizontal over the interval $[-0.8, 1.8]$, indicating a wide region of convergence and numerical stability. Selecting $p$ within this admissible range guarantees fast and reliable convergence of this method. Based on this analysis, the optimal value of the convergence parameter is chosen as $p=.32$. Fig. 9b presents a comparison between the zeroth- and first-order moment solutions obtained using the AMP method against the exact solutions. It can be easily seen that the AMP results exhibit excellent agreement with the exact solutions, confirming the accuracy and reliability of the proposed approach.

## 4. Concluding remarks and future aspects

The purpose of this work was to introduce a novel approximation method with a convergence acceleration parameter for solving a multi-dimensional aggregation population balance equation. The theoretical investigation for the convergence analysis of the method was carried out using the contractive mapping in the Banach space. A number of numerical problems are addressed to demonstrate the validity of this methodology and are compared to the recently developed homotopy analysis method and optimal decomposition method for a aggregation population balance equation. The convergence control parameter enables improving the series solutions for extended time frame by utilizing only a limited number of terms from the truncated series. This approach tackles the limitations found in existing methods such as the homotopy analysis method and optimal decomposition method. Additionally, the recently developed homotopy perturbation method necessitates the use of an extra Pade approximant tool to capture solutions over extended periods, resulting in increased computational complexity (Yadav et al., 2023).

The number density function and the zeroth and first order moments obtained by AMP exactly match with the exact moments and the existing finite volume scheme. The new series solutions for variety of physically relevant kernels corresponding to different exponential and Gamma initial conditions have been obtained. Given the superior accuracy and efficiency of the new approach, our next objective is to employ this technique to solve multidimensional population balance equations involving fragmentation, growth and nucleation mechanisms. This application will allow us to accurately capture various particle properties,

including size and liquid distributions. These properties are particularly relevant to crystallization and granulation processes within the chemical and pharmaceutical industries.

## CRediT authorship contribution statement

**Sonia Yadav:** Writing – review & editing, Writing – original draft, Visualization, Validation, Methodology, Investigation, Formal analysis, Conceptualization; **Akashdeep Singh:** Writing – review & editing, Writing – original draft, Visualization, Validation, Methodology, Investigation, Formal analysis, Conceptualization; **Sukhjit Singh:** Writing – review & editing, Visualization, Validation, Supervision, Methodology, Investigation, Formal analysis, Conceptualization; **Gavin Walker:** Writing – review & editing, Visualization, Investigation, Conceptualization; **Stefan Heinrich:** Writing – review & editing, Visualization, Validation, Formal analysis; **Rohit Ramachandran:** Writing – review & editing, Visualization, Validation, Investigation, Formal analysis; **Mehakpreet Singh:** Writing – review & editing, Writing – original draft, Visualization, Validation, Supervision, Project administration, Methodology, Investigation, Formal analysis, Conceptualization.

## Funding

This research received no specific grant from any funding agency in the public, commercial, or not-for-profit sectors.

## Declaration of competing interest

The authors declare that they have no known competing financial interests or personal relationships that could have appeared to influence the work reported in this paper.

## Data availability

No data was used for the research described in the article.

## Appendix A. Convergence analysis

Here, we discuss the convergence analysis of AMP for a nonlinear aggregation model. Let us introduce the Banach space $\mathbb{Y} = (C([0,\mathcal{T}] : \mathcal{L}^1[0,\infty)), \|.\|)$ with the norm (Stewart and Meister, 1989; Singh et al., 2015; Arora et al., 2024; Hussain and Kumar, 2024) defined as

$$\|\mu\| = \sup_{t\in[0,t_0]} \int_0^{\infty} |\mu(t,y)|dy \tag{A.1}$$

We demonstrate the existence of solutions to (1) by determining the limit of a series of approximation equations derived by substituting the kernel $\alpha$ by the "cut-off kernel $\alpha_k$ (Stewart and Meister, 1989) where

$$\alpha_k(y,z) = \begin{cases} \alpha(y,z) & \text{if} \quad y+z \le k \\ 0 & \text{if} \quad y+z > k \end{cases} \tag{A.2}$$

This restriction is only place to enforce the conservation of numerical method mathematically. It makes sure that no particles larger than $k$ are created during the aggregation process. However, this kernel condition will not be applied later while demonstrating the numerical approaches. The resulting equation of (1) written in the following form

$$\frac{\partial \mu^k(t,y)}{\partial t} = \frac{1}{2}\int_0^y \alpha_k(y-w,w)\mu^k(t,y-w)\mu^k(t,w)dw - \int_0^{k-y} \alpha_k(y,w)\mu^k(t,y)\mu^k(t,w)dw \tag{A.3}$$

with

$$\mu_0^k(y) = \begin{cases} \mu_0(y) & \text{if} \quad 0 \le y \le k \\ 0 & \text{if} \quad y > k. \end{cases} \tag{A.4}$$

and $\mu^k$ is the solution of (A.3). We will now prove the existence of the solutions $\mu^k(t,y)$ for each $k = 1,2,3,\ldots$

Choose $k \ge 1$ and $t_0 > 0, t \in [0,\infty)$. Let $\mathcal{K} = \max\{\alpha(y,w) : y,w \in (0,k)\}$. For $\mu^k \in (C([0,\mathcal{T}] : \mathcal{L}^1[0,k]), \|.\|)$ the norm is defined as

$$\|\mu^k\| = \sup_{t\in[0,t_0]} \int_0^k |\mu^k(t,y)|dy \tag{A.5}$$

Now, operate $\mathcal{L}^{-1}$ on both side of (A.3) and using (A.4), we get

$$\mu^k(t,y) = \mu_0^k(y) + \int_0^t \left[\frac{1}{2}\int_0^y \alpha_k(y-w,w)\mu^k(z,y-w)\mu^k(z,w)dw - \int_0^{k-y} \alpha_k(y,w)\mu^k(z,y)\mu^k(z,w)dw\right]dz \tag{A.6}$$

Let $S : \mathcal{Y} \to \mathcal{Y}$ be a linear operator defined as

$$S(\mu^k) = \mu_0^k(y) + \int_0^t \left[\frac{1}{2}\int_0^y \alpha_k(y-w,w)\mu^k(z,y-w)\mu^k(z,w)dw - \int_0^{k-y} \alpha_k(y,w)\mu^k(z,y)\mu^k(z,w)dw\right]dz. \tag{A.7}$$

Then, we can rewrite (A.6) in the following operator form as

$$\mu^k = S\mu^k \tag{A.8}$$

In the equivalent form, (A.6) can be written as

$$\frac{\partial}{\partial t}\left[\mu^k(t,y)e^{\mathcal{G}(y,t,\mu^k)}\right] = \frac{1}{2}e^{\mathcal{G}(y,t,\mu^k)}\int_0^y \alpha_k(y-w,w)\mu^k(t,y-w)\mu^k(t,w)dw \tag{A.9}$$

where $\mathcal{G}(y,t,\mu^k) = \int_0^t \int_0^{k-y} \alpha_k(y,w)\mu(z,w)dwdz$. We can rewrite (A.9) in the operator form as

$$\mu^k = \tilde{S}\mu^k \tag{A.10}$$

where

$$\tilde{S}\mu^k = \mu_0^k(y)e^{-\mathcal{G}(y,t,\mu^k)} + \frac{1}{2}\int_0^t e^{\mathcal{G}(y,z,\mu^k)-\mathcal{G}(y,t,\mu^k)} \int_0^y \alpha_k(y-w,w)\mu^k(z,y-w)\mu^k(z,w)dwdz \tag{A.11}$$

The operator $S$ and $\tilde{S}$ are equivalent so for the existence of solution of (A.8), it is enough to show the existence of solution of (A.10). To prove this we introduce some Lemmas which will used to show that $\tilde{S}$ has a fixed point by means of the contractive mapping principle.

**Lemma 1.** *For $\mu^k$, $\mu^{k^*} \in C([0,\mathcal{T}] : \mathcal{L}^1[0,k])$, we have for $0 \le z \le t \le t_0$ and $0 \le y \le k$,*

$$|\mathcal{A}(y,z,t)| \le (t-z)\mathcal{H}e^{(t-z)\mathcal{K}\mathcal{H}}\ \|\mu^k - \mu^{k^*}\| \tag{A.12}$$

*where* $\mathcal{H} = \max\{\|\mu^k\|, \|\mu^{k^*}\|\}$ *and* $\mathcal{A}(y,z,t) = e^{\mathcal{G}(y,z,\mu^k)-\mathcal{G}(y,t,\mu^k)} - e^{\mathcal{G}(y,z,\mu^{k^*})-\mathcal{G}(y,t,\mu^{k^*})}$

**Proof.** Let $\mathcal{G}(y,t,\mu^k) - \mathcal{G}(y,z,\mu^k) \ge \mathcal{G}(y,t,\mu^{k^*}) - \mathcal{G}(y,z,\mu^{k^*})$. Then, we have

$$\mathcal{A}(y,z,t) = -e^{-[\mathcal{G}(y,t,\mu^{k^*})-\mathcal{G}(y,z,\mu^{k^*})]}$$

$$\times\left[1-e^{\left\{-\{[\mathcal{G}(y,t,\mu^k)-\mathcal{G}(y,z,\mu^k)]-[\mathcal{G}(y,t,\mu^{k^*})-\mathcal{G}(y,z,\mu^{k^*})]\}\right\}}\right]$$

By using definition of $\mathcal{H}$, $\mathcal{K}$ and the inequality $1-e^{-y}\le y$ for $y\ge 0$, we have

$$\begin{aligned}|\mathcal{A}(y,z,t)| &\le -e^{-[\mathcal{G}(y,t,\mu^{k^*})-\mathcal{G}(y,z,\mu^{k^*})]}\big([\mathcal{G}(y,t,\mu^k)-\mathcal{G}(y,z,\mu^k)]\\ &\quad -[\mathcal{G}(y,t,\mu^{k^*})-\mathcal{G}(y,z,\mu^{k^*})]\big)\\ &= e^{\left(-\int_z^t\int_0^{k-y}\alpha_k(y,w)\mu^k(w,v)dwdv\right)}\\ &\quad\times\left|\int_z^t\int_0^{k-y}\alpha_k(y,w)(\mu^k(w,v)-\mu^{k^*}(w,v))dwdv\right|\\ &\le e^{\mathcal{K}\mathcal{H}(t-z)}\mathcal{K}(t-z)\|\mu^k-\mu^{k^*}\|\end{aligned}$$

If $\mathcal{G}(y,t,\mu^k)-\mathcal{G}(y,z,\mu^k)\le\mathcal{G}(y,t,\mu^{k^*})-\mathcal{G}(y,z,\mu^{k^*})$, then the same inequality (A.12) is obtained. □

Define $\mathcal{D}=\{\mu^k\in C([0,\mathcal{T}]:\mathcal{L}^1[0,k]):\|\mu^k\|\le 2\mathcal{N}\}$, where $\mathcal{N}=(1+\mathcal{T})\|\mu_0\|$

**Lemma 2.** *The operator $\mathcal{S}$ maps $\mathcal{D}$ to itself if $e^{2\mathcal{N}t\mathcal{K}}(1+2\mathcal{K}\mathcal{N}t)\le 2$*

**Proof.** Choose $\mu^k$ with $\|\mu^k\|\le 2\mathcal{N}$. Now, integrate (A.11) from 0 to $k$, we get

$$\begin{aligned}&\int_0^k|\tilde{\mathcal{S}}(\mu^k)(t,y)|dy=\int_0^k\left[\mu_0^k(y)e^{-\mathcal{G}(t,y,\mu^k)}+\frac{1}{2}\int_0^t e^{\mathcal{G}(z,y,\mu^k)-\mathcal{G}(t,y,\mu^k)}\right.\\ &\left.\int_0^y\alpha_k(y-w,w)\mu^k(z,y-w)\mu^k(z,w)dwdz\right]dy\\ &\le\|\mu_0^k\|e^{t\mathcal{K}\|\mu^k\|}+\frac{e^{(t\mathcal{K}\|\mu^k\|)}\mathcal{K}}{2}\int_0^k\int_0^t\int_0^y\mu^k(z,y-w)\mu^k(z,w)dwdzdy\end{aligned}$$

Substitute $y-w=v$ and interchange the integration limits, we get

$$\begin{aligned}\int_0^k|\tilde{\mathcal{S}}(\mu^k)(t,y)|dy &\le\|\mu_0^k\|e^{t\mathcal{K}\|\mu^k\|}\\ &\quad+\frac{e^{(t\mathcal{K}\|\mu^k\|)}\mathcal{K}}{2}\int_0^t\int_0^k\mu^k(z,w)\int_0^{k-w}\mu^k(z,v)dvdwdz\\ &\le\|\mu_0^k\|e^{t\mathcal{K}\|\mu^k\|}+\frac{e^{(t\mathcal{K}\|\mu^k\|)}\mathcal{K}}{2}\|\mu^k\|^2t\\ &\le e^{2\mathcal{N}t\mathcal{K}}(\|\mu_0^k\|+\mathcal{K}2\mathcal{N}^2t)\le\mathcal{N}e^{2\mathcal{N}t\mathcal{K}}(1+\mathcal{K}2\mathcal{N}t)\le 2\mathcal{N}\end{aligned}$$

Since $e^{2\mathcal{N}t\mathcal{K}}(1+2\mathcal{K}\mathcal{N}t)\le 2$. □

**Lemma 3.** *For $\mu^k,\mu^{k^*}\in\mathcal{N}$ there exists $\beta\in[0,1]$ such that*

$$\|\tilde{\mathcal{S}}(\mu^k)-\tilde{\mathcal{S}}(\mu^{k^*})\|\le\beta\|\mu^k-\mu^{k^*}\| \tag{A.13}$$

*with $\beta=t\mathcal{K}e^{2t\mathcal{K}\mathcal{N}}[\|\mu_0^k\|+2\mathcal{N}+2t\mathcal{N}\mathcal{K}]<1$*

**Proof.** Now, for any $\mu^k,\mu^{k^*}\in\mathcal{Y}_1$, we have

$$\begin{aligned}\tilde{\mathcal{S}}(\mu^k)-\tilde{\mathcal{S}}(\mu^{k^*}) &=\mu_0^k(y)\left[e^{-\mathcal{G}(y,t,\mu^k)}-e^{-\mathcal{G}(y,t,\mu^{k^*})}\right]+\frac{1}{2}\int_0^t e^{\mathcal{G}(y,z,\mu^k)-\mathcal{G}(y,t,\mu^k)}\\ &\quad\int_0^y\alpha(y-w,w)\mu^k(y-w,z)\mu^k(w,z)dwdz\\ &\quad-\frac{1}{2}\int_0^t e^{\mathcal{G}(y,z,\mu^{k^*})-\mathcal{G}(y,t,\mu^{k^*})}\\ &\quad\int_0^y\alpha(y-w,w)\mu^{k^*}(y-w,z)\mu^{k^*}(w,z)dwdz\\ &=\mu_0^k(y)\mathcal{A}(y,0,t)+\frac{1}{2}\int_0^t\mathcal{A}(y,z,t)\int_0^y\mu^k(y-w,z)\mu^k(w,z)\\ &\quad dwdz+\frac{1}{2}\int_0^t e^{\mathcal{G}(y,z,\mu^{k^*})-\mathcal{G}(y,t,\mu^{k^*})}\left[\int_0^y\mu^{k^*}(y-w,z)[\mu^k(w,z)\right.\\ &\quad-\mu^{k^*}(w,z)]dw\\ &\quad+\int_0^y\alpha(y-w,w)\mu^k(w,z)[\mu^k(y-w,z)\\ &\quad\left.-\mu^{k^*}(y-w,z)]dw\right]dz,\end{aligned}$$

By using Lemma 1 and Lemma 2 and taking norm on both side, we get the following inequality

$$\begin{aligned}\|\tilde{\mathcal{S}}(\mu^k)-\tilde{\mathcal{S}}(\mu^{k^*})\| &\le\mathcal{K}te^{2t\mathcal{K}\mathcal{N}}\|\mu_0^k\|\|\mu^k-\mu^{k^*}\|+t\mathcal{K}e^{2t\mathcal{K}\mathcal{N}}\|\mu^k\\ &\quad-\mu^{k^*}\|\left(\frac{\mathcal{K}}{2}4\mathcal{N}^2\right)t+te^{2t\mathcal{K}\mathcal{N}}\left(\frac{\mathcal{K}}{2}2\mathcal{N}+\frac{\mathcal{K}}{2}2\mathcal{N}\right)\\ &\le t\mathcal{K}e^{2t\mathcal{K}\mathcal{N}}[3\mathcal{N}+2t\mathcal{N}\mathcal{K}]\|\mu^k-\mu^{k^*}\|=\beta\|\mu^k-\mu^{k^*}\|\end{aligned}$$

where $\beta=t\mathcal{K}e^{2t\mathcal{K}\mathcal{N}}[3\mathcal{N}+2t\mathcal{N}\mathcal{K}]<1$. Thus, for each $k=1,2,3\ldots$ (A.3)-(A.4) has a solution. □

If we consider the truncated equation defined in (A.3) with initial condition (A.4), then by formulation using AMP, we get the following recurrence relation

$$\begin{cases}\mu_0^k(y) & \text{given}\\ \mu_1^k(t,y,p)=p\int_0^t\left[\frac{1}{2}\int_0^y\alpha(y-w,w)\mathcal{P}_0^k(\mu)dw-\int_0^{k-y}\alpha(y,w)\mathcal{Q}_0^k(\mu)dw\right]dt\\ \mu_m^k(t,y,p)=(1-p)\\ \int_0^t\left[\frac{1}{2}\int_0^y\alpha(y-w,w)\mathcal{P}_{m-2}^k(\mu)dw-\int_0^{k-y}\alpha(y,w)\mathcal{Q}_{m-2}^k(\mu)dw\right]dt\\ +p\int_0^t\left[\frac{1}{2}\int_0^y\alpha(y-w,w)\mathcal{P}_{m-1}^k(\mu)dw-\int_0^{k-y}\alpha(y,w)\mathcal{Q}_{m-1}^k(\mu)dw\right]dt\end{cases} \tag{A.14}$$

where $\mathcal{P}_m^k=\frac{1}{m!}\frac{d^m}{dv^m}\left[h_1\left(\sum_{n=0}^{\infty}\mu_n^kv^n\right)\right]_{v=0}$ and $\mathcal{Q}_m^k=\frac{1}{m!}\frac{d^m}{dv^m}\left[h_2\left(\sum_{n=0}^{\infty}\mu_n^kv^n\right)\right]_{v=0}$.

The $r$th- order truncated approximation solution is given by

$$\vartheta_r^k(t,y,p)=\sum_{m=0}^r\mu_m^k(t,y,p),\qquad r\ge 1 \tag{A.15}$$

**Theorem 1.** *Suppose $\mu_0^k,\mu_1^k,\ldots$ are the components of the iterative method (A.14) and $\vartheta_r^k(t,y,p)$ be the rth term series solution defined in (A.15). Then, the series solution $\vartheta_r^k(t,y,p)=\sum_{m=0}^r\mu_m^k(t,y,p)$ converges to the solution with*

1. *For all $y,z\in[0,k]$, we consider*

$$\alpha_k(y,z)=\begin{cases}\alpha(y,z) & \text{if}\quad y+z\le k\\ 0 & \text{if}\quad y+z>k\end{cases}$$

*and $\mathcal{K}=\max\{\alpha(y,w):y,w\in(0,k)\}$.*

2. *For $\mu^k,\mu^{k^*}\in C([0,\mathcal{T}]:\mathcal{L}^1[0,k])$, if $\|\mathcal{S}(\mu^k)-\mathcal{S}(\mu^{k^*})\|\le\beta_1\|\mu^k-\mu^{k^*}\|$, $e^{2\mathcal{N}t\mathcal{K}}(1+2\mathcal{K}\mathcal{N}t)\le 2$ and $\beta_1=t\mathcal{K}e^{2t\mathcal{K}\mathcal{N}}[\|3\mathcal{N}+2t\mathcal{N}\mathcal{K}]<1$, where $\mathcal{N}=(1+\mathcal{T})\|\mu_0\|$.*

**Proof.** Now, from (A.14) and (A.15), we get

$$\vartheta_r^k(t,y,p)=\sum_{m=0}^y\mu_m^k(t,y)=\mu_0^k(y)+p\left(\int_0^t\left[\frac{1}{2}\int_0^y\alpha_k(y-w,w)\mathcal{P}_1^k(\mu)dw\right.\right.$$

$$
\begin{aligned}
&- \int_0^{k-y} \alpha_k(y,w)\mathcal{Q}_1^k(\mu)dw\Bigg]dt\Bigg) \\
&+ \sum_{m=2}^{r}(1-p)\int_0^t\left[\frac{1}{2}\int_0^y \alpha_k(y-w,w)\mathcal{P}_{m-2}^k(\mu)dw\right. \\
&\left.- \int_0^{k-y} \alpha_k(y,w)\mathcal{Q}_{m-2}^k(\mu)dw\right]dt \\
&+ p\int_0^t\left[\frac{1}{2}\int_0^y \alpha_k(y-w,w)\mathcal{P}_{m-1}^k(\mu)dw - \int_0^{k-y} \alpha_k(y,w)\mathcal{Q}_{m-1}^k(\mu)dw\right] \\
&= \mu_0^k(y) + p\Bigg(\int_0^t\left[\frac{1}{2}\int_0^y \alpha_k(y-w,w)\sum_{m=0}^{r-1}\mathcal{P}_m^k(\mu)dw\right. \\
&\left.- \int_0^{k-y} \alpha_k(y,w)\sum_{m=0}^{r-1}\mathcal{Q}_m^k(\mu)dw\right]dt\Bigg) \\
&+ (1-p)\int_0^t\left[\frac{1}{2}\int_0^y \alpha_k(y-w,w)\sum_{m=0}^{r-2}\mathcal{P}_m^k(\mu)dw\right. \\
&\left.- \int_0^{k-y} \alpha_k(y,w)\sum_{m=0}^{r-2}\mathcal{Q}_m^k(\mu)dw\right]dt \\
&= p\Bigg(\mu_0^k(y) + \int_0^t\left[\frac{1}{2}\int_0^y \alpha_k(y-w,w)h_1(\vartheta_{r-1}^k)dw\right. \\
&\left.- \int_0^{k-y} \alpha_k(y,w)h_2(\vartheta_{r-1}^k)dw\right]dt\Bigg) \\
&+ (1-p)\int_0^t\left[\mu_0^k(y) + \frac{1}{2}\int_0^y \alpha_k(y-w,w)h_1(\vartheta_{r-2}^k)dw\right. \\
&\left.- \int_0^{k-y} \alpha_k(y,w)h_2(\vartheta_{r-2}^k)dw\right]dt \\
&= pS(\vartheta_{r-1}^k) + (1-p)S(\vartheta_{r-2}^k) \qquad \text{(A.16)}
\end{aligned}
$$

In addition, we have

$$
\begin{aligned}
\|\vartheta_{r+1}^k - \vartheta_r^k\| &\le p\,\|S(\vartheta_r^k) - S(\vartheta_{r-1}^k)\| + |1-p|\,\|S(\vartheta_{r-1}^k) - S(\vartheta_{r-2}^k)\| \\
&\le p\beta_1\,\|\vartheta_r^k - \vartheta_{r-1}^k\| + |1-p|\,\beta_1\,\|\vartheta_{r-1}^k - \vartheta_{r-2}^k\| \\
&\le (p\beta_1^r + |1-p|\beta_1^{r-1})\|\vartheta_1^k - \vartheta_0^k\| = \gamma\|\vartheta_1^k - \vartheta_0^k\|
\end{aligned}
$$

where $\gamma = p\beta_1^r + |1-p|\beta_1^{r-1} < 1$, since $\beta_1 < 1$ and $p \in [0,1]$. Now, for all $r,t \in \mathbb{N}$ with $t \le r$, we get

$$
\begin{aligned}
\|\vartheta_r^k - \vartheta_t^k\| &\le \|\vartheta_r^k - \vartheta_{r-1}^k\| + \|\vartheta_{r-1}^k - \vartheta_{r-2}^k\| + \ldots + \|\vartheta_{t+1}^k - \vartheta_t^k\| \\
&\le [\gamma^{r-1} + \gamma^{r-2} + \ldots + \gamma^t]\|\vartheta_1^k - \vartheta_0^k\| \\
&= \gamma^t[1 + \gamma + \gamma^2 + \ldots + \gamma^{r-t-1}]\|\vartheta_1^k - \vartheta_0^k\| \\
&= \gamma^t\left(\frac{1-\gamma^{r-t}}{1-\gamma}\right)\|\mu_1^k\|.
\end{aligned}
$$

It follows that

$$
\|\vartheta_r^k - \vartheta_t^k\| \le \frac{\gamma^t}{1-\gamma}\|\mu_1^k\|, \qquad \text{(A.17)}
$$

which converges to zero as $t \to \infty$, since $0 < \gamma < 1$. As a result, $\{\vartheta_r^k\}$ is Cauchy sequence in $(C([0,\mathcal{T}] : \mathcal{L}^1[0,k]), \|.\|)$, hence it must be convergent. Let there exist $\vartheta^k$ in $(C([0,\mathcal{T}] : \mathcal{L}^1[0,k]), \|.\|)$ such that $\lim_{r\to\infty}\vartheta_r^k = \vartheta^k$. But we have $\mu^k = \sum_{m=0}^{\infty}\mu_m = \lim_{r\to\infty}\vartheta_r^k = \vartheta^k$ which is the exact solution of truncated problem (A.3). □

**Theorem 2.** *Let $\mu^k$ be the exact solution of (A.3) and $\vartheta_r^k$ be the series solution (A.15), then*

$$
\|\mu^k - \vartheta_r^k\| \le \frac{\gamma^j}{(1-\gamma)}\|\mu_1\|, \qquad \text{(A.18)}
$$

*where* $\|\mu_1\| = \sup_{t\in[0,\mathcal{T}]}\int_0^k |\mu_1(t,r)|\,dr$.

**Proof.** From (A.17), for $r \ge t$, where $r,t \in \mathbb{N}$, we have

$$
\|\vartheta_r^k - \vartheta_t^k\| \le \frac{\gamma^t}{(1-\gamma)}\|\mu_1^k\|.
$$

Since $\lim_{r\to\infty}\vartheta_r^k = \mu^k$, fixing $t$ and taking $r \to \infty$ in above estimate, the desired result is obtained. □

## References


Ahrens, R., Le Borne, S., 2018. Fft-based evaluation of multivariate aggregation integrals in population balance equations on uniform tensor grids. J. Comput. Appl. Math. 338, 280–297.

Aldous, D.J., 1999. Deterministic and stochastic models for coalescence (aggregation and coagulation): a review of the mean-field theory for probabilists. Bernoulli , 3–48.

Ami, R.B., Barshtein, G., Zeltser, D., Goldberg, Y., Shapira, I., Roth, A., Keren, G., Miller, H., Prochorov, V., Eldor, A., et al., 2001. Parameters of red blood cell aggregation as correlates of the inflammatory state. Am. J. Physiol.-Heart Circ. Physiol. 280 (5), H1982–H1988.

Arora, G., Hussain, S., Kumar, R., 2023. Comparison of variational iteration and Adomian decomposition methods to solve growth, aggregation and aggregation-breakage equations. J. Comput. Sci. 67, 101973.

Arora, G., Kumar, R., Mammeri, Y., 2024. Elzaki transform based accelerated homotopy perturbation method for multi-dimensional smoluchowski's coagulation and coupled coagulation-fragmentation equations. J. Appl. Anal. Comput. 14 (5), 2922–2953.

Briesen, H., 2006. Simulation of crystal size and shape by means of a reduced two-dimensional population balance model. Chem. Eng. Sci. 61 (1), 104–112.

Chaudhury, A., Niziolek, A., Ramachandran, R., 2013. Multi-dimensional mechanistic modeling of fluid bed granulation processes: an integrated approach. Adv. Powder Technol. 24 (1), 113–131.

Das, P., Rana, S., Ramos, H., 2020a. A perturbation-based approach for solving fractional-order volterra–fredholm integro differential equations and its convergence analysis. Int. J. Comput. Math. 97 (10), 1994–2014.

Das, P., Rana, S., Vigo-Aguiar, J., 2020b. Higher order accurate approximations on equidistributed meshes for boundary layer originated mixed type reaction diffusion systems with multiple scale nature. Appl. Numer. Math. 148, 79–97.

Erabit, N., Ndoye, F.T., Alvarez, G., Flick, D., 2016. Coupling population balance model and residence time distribution for pilot-scale modelling of $\beta$-lactoglobulin aggregation process. J. Food Eng. 177, 31–41.

Fernandez-Diaz, J.M., Gomez-Garcia, G.J., 2007. Exact solution of smoluchowski's continuous multi-component equation with an additive kernel. Europhys. Lett. 78 (5), 56002.

Filbet, F., Laurençot, P., 2004. Numerical simulation of the smoluchowski coagulation equation. SIAM J. Sci. Comput. 25 (6), 2004–2028.

Forestier-Coste, L., Mancini, S., 2012. A finite volume preserving scheme on nonuniform meshes and for multidimensional coalescence. SIAM J. Sci. Comput. 34 (6), B840–B860.

Gelbard, F.M., Seinfeld, J.H., 1978. Coagulation and growth of a multicomponent aerosol. J. Colloid Interface Sci. 63 (3), 472–479.

Giri, A.K., Hausenblas, E., 2013. Convergence analysis of sectional methods for solving aggregation population balance equations: the fixed pivot technique. Nonlinear Anal.: Real World Appl. 14 (6), 2068–2090.

Gunawan, R., Fusman, I., Braatz, R.D., 2004. High resolution algorithms for multidimensional population balance equations. AIChE J. 50 (11), 2738–2749.

Hammouch, Z., Mekkaoui, T., 2012. A laplace-variational iteration method for solving the homogeneous smoluchowski coagulation equation. Appl. Math. Sci. 6 (18), 879–886.

Hussain, M., Kumar, J., Peglow, M., Tsotsas, E., 2014. On two-compartment population balance modeling of spray fluidized bed agglomeration. Comput. Chem. Eng. 61, 185–202.

Hussain, S., Kumar, R., 2024. Elzaki projected differential transform method for multi-dimensional aggregation and combined aggregation-breakage equations. J. Comput. Sci. 75, 102211.

Ismail, H.Y., Shirazian, S., Singh, M., Whitaker, D., Albadarin, A.B., Walker, G.M., 2020a. Compartmental approach for modelling twin-screw granulation using population balances. Int. J. Pharm. 576, 118737.

Ismail, H.Y., Singh, M., Shirazian, S., Albadarin, A.B., Walker, G.M., 2020b. Development of high-performance hybrid ann-finite volume scheme (ann-fvs) for simulation of pharmaceutical continuous granulation. Chem. Eng. Res. Des. 163, 320–326.

Kaur, G., Singh, R., Briesen, H., 2022. Approximate solutions of aggregation and breakage population balance equations. J. Math. Anal. Appl. 512 (2), 126166.

Kaur, G., Singh, R., Singh, M., Kumar, J., Matsoukas, T., 2019. Analytical approach for solving population balances: a Homotopy perturbation method. J. Phys. A: Math. Theor. 52 (38), 385201.

Kaushik, S., Kumar, R., 2023. A novel optimized decomposition method for Smoluchowski's aggregation equation. J. Comput. Appl. Math. 419, 114710.

Kobayashi, H., Tanaka, H., 2021. Rapid formation of gas-giant planets via collisional coagulation from dust grains to planetary cores. Astrophys. J. 922 (1), 16.
Kumar, J., Kaur, G., Tsotsas, E., 2016. An accurate and efficient discrete formulation of aggregation population balance equation. Kinet. Relat. Models 9 (2).
Kumar, J., Warnecke, G., 2008. Convergence analysis of sectional methods for solving breakage population balance equations-II: the cell average technique. Numer. Math. 110, 539–559.
Kumar, S., Das, P., Kumar, K., 2024a. Adaptive mesh based efficient approximations for darcy scale precipitation–dissolution models in porous media. Int. J. Numer. Methods Fluids 96 (8), 1415–1444.
Kumar, S., R, I., Das, P., 2024b. Impact of mixed boundary conditions and nonsmooth data on layer-originated nonpremixed combustion problems: higher-order convergence analysis. Stud. Appl. Math. 153 (4), e12763.
Kushwah, P., Saha, J., 2023. Improved accuracy and convergence of homotopy-based solutions for aggregation–fragmentation models. Math. Methods Appl. Sci. 46 (6), 7180–7200.
Liu, A., Rigopoulos, S., 2019. A conservative method for numerical solution of the population balance equation, and application to soot formation. Combust. Flame 205, 506–521.
Marchisio, D.L., Vigil, R.D., Fox, R.O., 2003. Quadrature method of moments for aggregation–breakage processes. J. Colloid Interface Sci. 258 (2), 322–334.
Matveev, S.A., Smirnov, A.P., Tyrtyshnikov, E.E., 2015. A fast numerical method for the cauchy problem for the smoluchowski equation. J. Comput. Phys. 282, 23–32.
McMahon, D.J., Brown, R.J., 1984. Enzymic coagulation of casein micelles: a review. J. Dairy Sci. 67 (5), 919–929.
Mostafaei, P., Rajabi-Hamane, M., 2017. Numerical solution of the population balance equation using an efficiently modified cell average technique. Comput. Chem. Eng. 96, 33–41.
Payens, T.A., 1989. The enzyme-triggered coagulation of casein micelles. Adv. Colloid Interface Sci. 30, 31–69.
Qamar, S., Warnecke, G., 2007. Solving population balance equations for two-component aggregation by a finite volume scheme. Chem. Eng. Sci. 62 (3), 679–693.
Ranjbar, M., Adibi, H., Lakestani, M., 2010. Numerical solution of homogeneous smoluchowski's coagulation equation. Int. J. Comput. Math. 87 (9), 2113–2122.
Saini, S., Das, P., Kumar, S., 2023. Computational cost reduction for coupled system of multiple scale reaction diffusion problems with mixed type boundary conditions having boundary layers. Revista de la Real Academia de Ciencias Exactas, Físicas y Naturales. Serie A. Matemáticas 117 (2), 66.
Saini, S., Das, P., Kumar, S., 2024. Parameter uniform higher order numerical treatment for singularly perturbed robin type parabolic reaction diffusion multiple scale problems with large delay in time. Appl. Numer. Math. 196, 1–21.
Santra, S., Das, P., Jorgensen, P., 2025. A unified multifaceted space-time wavelet framework and its singularity analysis for weakly singular non-local partial integro-differential equations in high dimensions. Acta Appl. Math. 200 (1), 1–42.
Santra, S., Mohapatra, J., Das, P., Choudhuri, D., 2023. Higher order approximations for fractional order integro-parabolic partial differential equations on an adaptive mesh with error analysis. Comput. Math. Appl. 150, 87–101.
Scott, W.T., 1968. Analytic studies of cloud droplet coalescence i. J. Atmos. Sci. 25 (1), 54–65.
Shirazian, S., Ismail, H.Y., Singh, M., Shaikh, R., Croker, D.M., Walker, G.M., 2019. Multidimensional population balance modelling of pharmaceutical formulations for continuous twin-screw wet granulation: determination of liquid distribution. Int. J. Pharm. 566, 352–360.
Singh, M., 2021. New finite volume approach for multidimensional smoluchowski equation on nonuniform grids. Stud. Appl. Math. 147 (3), 955–977.
Singh, M., 2023. Rate of convergence of two moments consistent finite volume scheme for non-classical divergence coagulation equation. Appl. Numer. Math. 187, 120–137.
Singh, M., Nayak, R.K., Walker, G., 2022a. Convergence analysis of volume preserving scheme for mass based coalescence equation. Appl. Numer. Math. 173, 365–379.
Singh, M., Ranade, V., Shardt, O., Matsoukas, T., 2022b. Challenges and opportunities concerning numerical solutions for population balances: a critical review. J. Phys. a: Math. Theor. 55 (38), 383002.
Singh, M., Shirazian, S., Ranade, V., Walker, G.M., Kumar, A., 2022c. Challenges and opportunities in modelling wet granulation in pharmaceutical industry–a critical review. Powder Technol. , 117380.
Singh, M., Singh, R., Singh, S., Walker, G., Matsoukas, T., 2020. Discrete finite volume approach for multidimensional agglomeration population balance equation on unstructured grid. Powder Technol. 376, 229–240.
Singh, R., Saha, J., Kumar, J., 2015. Adomian decomposition method for solving fragmentation and aggregation population balance equations. J. Appl. Math. Comput. 48, 265–292.
Smoluchowski, M.V., 1917. Mathematical theory of the kinetics of the coagulation of colloidal solutions. Z. f'ur Phys. Chemi 92, 129–168.
Stewart, I.W., Meister, E., 1989. A global existence theorem for the general coagulation–fragmentation equation with unbounded kernels. Math. Methods Appl. Sci. 11 (5), 627–648.
Turkyilmazoglu, M., 2016. Convergent optimal variational iteration method and applications to heat and fluid flow problems. Int. J. Numer. Methods Heat Fluid Flow 26 (3–4), 790–804.
Turkyilmazoglu, M., 2018. A reliable convergent adomian decomposition method for heat transfer through extended surfaces. Int. J. Numer. Methods Heat Fluid Flow 28 (11), 2551–2566.
Turkyilmazoglu, M., 2022. An efficient computational method for differential equations of fractional type. Comput. Model. Eng. Sci. 133 (1).
Turkyilmazoglu, M., 2024. Optimization by the convergence control parameter in iterative methods. J. Appl. Math. Comput. Mech. 23 (2).
Vale, H.M., McKenna, T.F., 2005. Solution of the population balance equation for two-component aggregation by an extended fixed pivot technique. Ind. Eng. Chem. Res. 44 (20), 7885–7891.
Wang, L.G., Ge, R., Chen, X., Zhou, R., Chen, H.-M., 2021. Multiscale digital twin for particle breakage in milling: from nanoindentation to population balance model. Powder Technol. 386, 247–261.
Xue, Y., Wang, L.-P., Grabowski, W.W., 2008. Growth of cloud droplets by turbulent collision–coalescence. J. Atmos. Sci. 65 (2), 331–356.
Yadav, N., Singh, M., Singh, S., Singh, R., Kumar, J., 2023. A note on homotopy perturbation approach for nonlinear coagulation equation to improve series solutions for longer times. Chaos Solit. Fractals 173, 113628.
Zhang, X., Zou, L., Liang, S., Liu, C., 2018. A novel analytic approximation method with a convergence acceleration parameter for solving nonlinear problems. Commun. Nonlinear Sci. Numer. Simul. 56, 354–364.